Deanship of Graduate Studies
Al- Quds University

H^+ outflow in the polar wind: A comparative study between RCC, Bouhram, Barghouthi models and observations

Sa'ed Rajab Mousa Shaheen

M.Sc. Thesis

Jerusalem-Palestine

1432 / 2011

H^+ outflow in the polar wind: A comparative study between RCC, Bouhram, Barghouthi models and observations

Prepared By:

Sa'ed Ragab Musa Shahin

B.Sc: Physics (An-Najah national university) (Palestine)

Supervisor: **Prof. Dr. Imad A. Barghouthi**

A thesis Submitted in Partial fulfillment of requirement for the degree of Master of Science in Physics
Department/Physics Master

Faculty of Science/Al- Quds University

1432 / 2011

Al-Quds University
Deanship of Graduate Studies
Master of Physics / Physics Department

Thesis Approval

H^+ outflow in the polar wind: A comparative study between RCC, Bouhram, Barghouthi models and observations

Prepared by : Sa'ed Rajab Mousa Shaheen
Registration No : 20610265

Supervisor: Prof. Dr. Imad A. Barghouthi

Master thesis submitted and accepted, Date: 21/5/2011
The names and signatures of the examining committee members are as follows

1. **Prof. Imad A. Barghouthi** **Signature…….**
2. **Prof. Mohammad I. Abu-Taha** **Signature…….**
3. **Dr. Mustafa Abu Safa** **Signature…….**

Jerusalem-Palestine

1432 / 2011

بسم الله الرحمن الرحيم

رَبِّ اشْرَحْ لِي صَدْرِي وَيَسِّرْ لِي أَمْرِي وَاحْلُلْ عُقْدَةً مِّن لِّسَانِي يَفْقَهُوا قَوْلِي

Dedication

To my parents, for their breeding and supporting, trying to back a driblet of their favor.

And to my family, my wife for her patience, and my sons encouraging them to walk in science road.

Sa’ed Ragab Musa Shahin

Declaration

I hereby declare that the entire work of this thesis has been carried out by me under the supervision of Prof. Dr. Imad A. Barghouthi, Department of physics – Faculty of science at Al- Quds University, and this thesis or any part of the same has not been submitted for any other university or institution except the acknowledged parts.

Signed …….

Sa'ed Rajab Mousa Shaheen

Date : 21/5/2011

Telephone : 00972-02-2235028

00972-02-2231232

Mobile : 00972-0569758801

00972-0599758801

E-mail : s11sh@yahoo.com

saedrsh@hotmail.com

Acknowledgements

First, thanks for Allah, who supported me with hope and power to do my studies without dereliction in my job or my family duties, I express my sincere gratitude to my university Al Quds University and the physics staff specially my supervisor Prof. Dr. Imad A. Barghouthi, for his valuable guidance and suggestions during the work, and Prof. Dr. Abdelkarim M. Saleh who is a faithful scientist example for me, and all physics staff members which forming a preferential department.

I thank my colleague Mr Sharif Ghithan for his assistant and sustaining, and for my colleague Ms Shayma' Ghanem, and for everyone who helped me in this work.

My family is the base of my ambition, and the place where I spent a lot of time to do my thesis is between them and by their help, specially my father, mother, and my wife.

Abstract:

One of the most important solar- terrestrial interaction results is ion outflow at high altitudes and latitudes regions as Aurora and Polar wind, so several models have been suggested to investigate the behavior of ion outflows, the energization mechanism for charged particles like H^+ to outflow is a subject of controversy, one important mechanism is the perpendicular heating by wave particle interaction (i.e. ion interactions with electromagnetic turbulences). Suggestion of perpendicular wavelength effects in the wave-particle interaction mechanism was reported by many researches as [Chang and Coppi, 1981], [Retterer et al., 1987a, 1987b, 1994], [Barghouthi, 1997; Barghouthi et al., 1998] and [Bouhram et al., 2003a, 2003b, 2004]. Velocity and altitude dependent $D_\perp$ was used in simulation as a combined of altitude part from [Barghouthi, 1997] and velocity part from [Bouhram et al., 2004], a comparison was made between the results of the three models (Barghouthi, Bouhram and RCC) at Polar wind region for hydrogen ion H^+, Monte Carlo Method was used in computer simulation include the effect of altitude-velocity wave particle interaction, polarization electrostatic field, gravity, and the divergence geomagnetic field. The simulation starts from 1.7 Re altitude to 13.7 Re as a simulation tube, with many important observed parameters at the lower boundary where the distribution function assumed to be Maxwellian. The results gives the effect of velocity dependent wave particle interaction by formation of conic and toroidal shape for velocity distribution function, and gives the lower order moments for H^+ , density, velocity , parallel and perpendicular velocities. The comparison showed closed between Barghouthi and Bouhram models and more strong wave particle interaction in RCC model, and the Aurora results show high velocities and temperatures for particles by strong perpendicular heating and more electromagnetic wave turbulences.

Table of contents

List of figures

List of Abbreviations

RCC: Retterer, Crew and Chang

Fig. : Figure.

WPI: Wave Particle Interaction.

IMF: Interplanetary Magnetic Field

AU: Astronomical Unit

UV: Ultra Violet

EUV: Extreme Ultra Violet

DE-1: Dynamic Explorer 1 satellite

PWI: Plasma Wave Instrument

Chapter One

Introduction

(wide view)

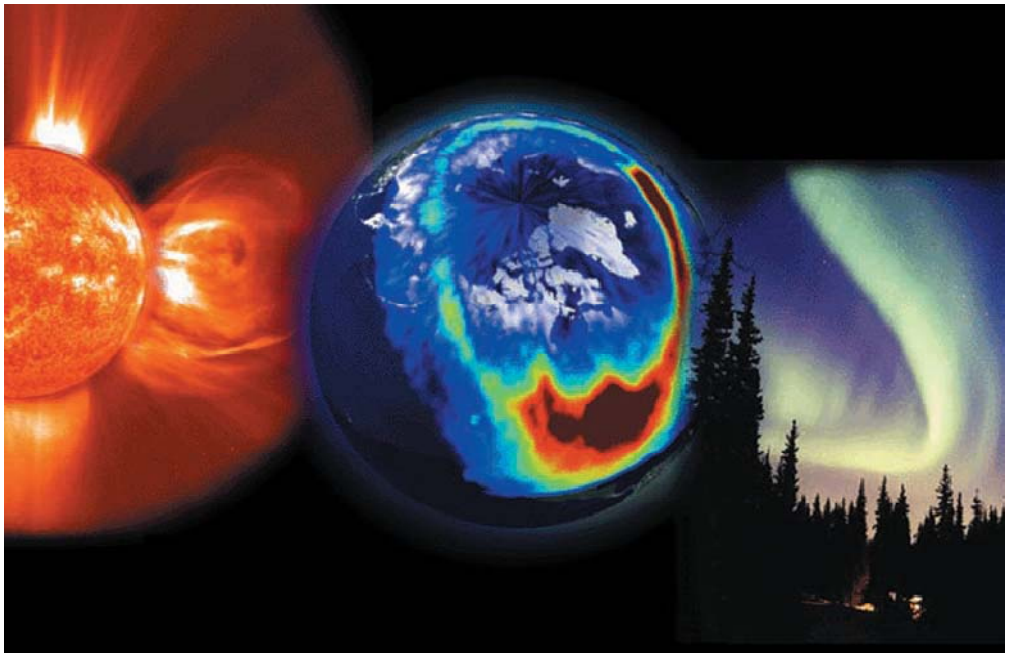

1.1 Introduction

The study will deal with the behavior of the H^+ ions outflow at high altitudes and latitudes (polar region) under the effect of many forces. This phenomena occurs under the effect of sun activities, which is the source of most energetic phenomena on our planet. The study is also one of these activities, the connection between the sun and it's planet earth does not only involve gravity and electromagnetic spectrum, but also concern the plasma which consists of ions and electrons (solar wind and coronal mass ejection) which encounter the planet.

The first attention for solar-terrestrial connection was by the British scientists Richard Carrington at 1859 when he observed brightening sunspot (sun flare) while he is sketching sunspots, and during several days after his observations the aurora being active and the telegraph system suffered in operation, now the relation between sun's activity and our planet is more clear.

The chapter will be presented in wide view from the sun for it's importance and centric, then the solar wind, the interaction between the solar wind and our planet (solar – terrestrial interaction), step by step to reach the polar wind and the factors which control this process and the behavior of plasma, specially the effect of wave particle interaction.

1.2 The sun

Sun is the source of polar phenomena, so understanding this star will help to understand the polar ion outflow within a complete puzzle. The sun is the central body in our solar system, formed before 5 billion years ago consists of 70.7% hydrogen (by mass), 27.4% helium and 1.9% other heavier elements. The sun is the main source of energy to planet earth and the dynamo of the life. It is a magnetic star, represents a typical star in our galaxy, rotate every 27 earth's day, and the sun with heliosphere move relative to interstellar medium in 23 Km/s. Studying the sun is important for us because it's a big and closed plasma physics laboratory, magneto-hydrodynamics (MHD), nuclear physics, and particle physics. Only this star can be seen in many wavelengths.

Table 1.1: Basic Physical Properties of the Sun (Encyclopedia of the solar system, Source: [Cox, 2000].

Solar radius	695,500 km		Mean distance from Earth	1 AU = 149,597,870 km
Solar mass	1.989×10^{33} g		Solar age	4.57×10^{9} years
Mean density	1.409 g cm^{-3}		Temperature at Sun center	15.7×10^{6} K
Gravity at solar surface	274.0 m s^{-2}		Temperature at solar surface	6400 K

The source of solar energy was understood in the 1920s, nearly 8% of the hydrogen burned into the helium by the nuclear reaction in the central core where the temperature is nearly 15 million K. Radiation accompany transformation of hydrogen to helium hence converts 0.7% of the mass according to energy-mass equivalence. [Elkins -Tanton, 2006].

The sun divided into two main parts; the interior and the atmosphere. The solar interior consist of: the core, radiative zone, and the convection zone. The solar atmosphere contain the photosphere, the chromosphere, a transition region, and the corona, after the corona there is outward flow of coronal gas which called the solar wind, look at Fig. (1.1).

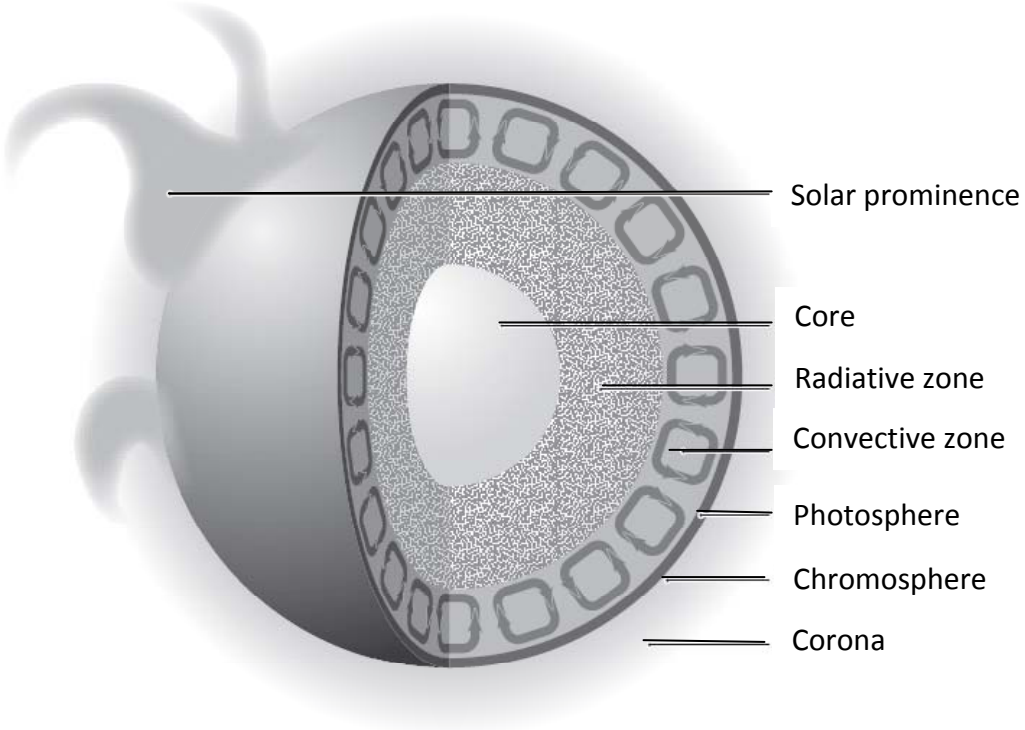

Figure 1.1: The sun anatomy internal structure of the sun, from the inner core to the external atmosphere (Corona), [Elkins-Tanton, 2006].

The magnetic dynamo processes which occur within convection zone turbulences generates the sun's magnetic field, this magnetic field emerge from beneath of the photosphere, the magnetic flux tubes rise through the convection zone and emerge at the surface in the active regions and form sunspots and coronal loops. The differential rotation on the solar surface will wind up the surface magnetic field which will fragment under the magnetic stress, [Lucy-Ann McFadden et al., 2007].

The solar dynamo flip the magnetic polarity of the sun every 11 years, and 22 year to cycle the global magnetic activity when it returns to the same magnetic configuration (the earth flip it's polarity also but over time of hundreds of thousands to millions of years), this solar cycle controls the rate of the solar activities like the number of sun spots, flares and coronal mass ejection (CME), because all of the solar activities are controlled by the magnetic field, so all the solar activity phenomena have a similar cycle like number of sunspots, also many terrestrial phenomena like Aurora.

The number of sunspots increase and decrease in a repeatable cycle, at the solar minimum conditions the sunspots number are few (may be fewer than 5 spots) here the sun like large bar magnet with north and south poles, and the sunspots begin at latitudes about 30^{o} in both hemispheres, the spots migrate toward the equator (sun's poles migrate) and the number of solar spots increases (may reach 250 spots) that is make the magnetic field configuration is very difficult at the solar maximum conditions, [Leif J. Robinson, 2002].

The magnetic flux creation supposed to be between the radiative zone and the convection zone which is known as the tachocline, this layer separate the uniform rotation region from differential rotation region, at the surface the strongest magnetic flux tubes destroy the granulation pattern and emerge within the sunspots, that make an inhibition for convection transport of heat, and decreases the heat emitting at the surface (darker than the surround as in Fig. (1.2) making a significantly cooler (4500 K) than the surroundings (6000 K), the range of their diameters from 3600 to 50,000 km, and the lifetime range from a week to several months, [Lucy-Ann McFadden et al., 2007].

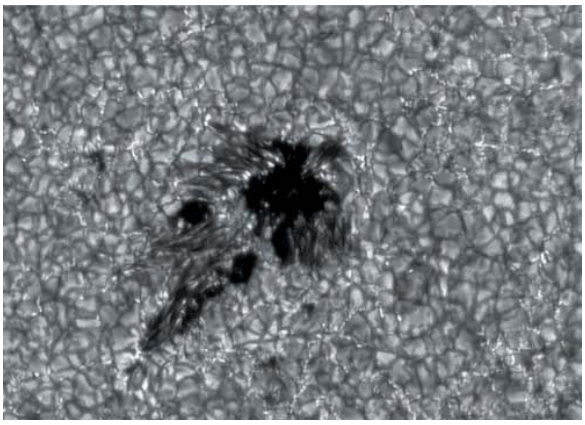

Image 1.1: the granulation pattern in the solar photosphere. A granule has a typical size of 1000 km, forming the elementary convection cell of the sun's surface, we can see the sunspot (The large black area), the temperature of the sunspot is cooler than the surroundings, this image by Tom Berger with The Institute for Solar Physics, http://www.solarphysics.kva.se (2011).

1.3 The solar wind

The solar wind is a charged particles ejected as a supersonic expansion of solar corona (sun's outer atmosphere), the solar wind consists of electrons and ions (most are protons with small abundance of alpha particles and other), Till now it's not fully understood how the solar corona is heated to high temperature and how the solar wind accelerated, [The Sun to the Earth -- and Beyond, National Research Council, 2003].

To browse the mean value of some important statistical properties for the solar wind by spacecraft measurements away from the sun one astronomical unit (Encyclopedia of the solar system, 2nd edition 2007). For **proton** density is 8.7 /cm^3, the flow speed 468 km/s , magnetic field strength 6.2 nT, proton temperature is 1.2×10^5 K, and electron temperature is 1.4×10^5 K , But the solar wind is highly variable in space and time.

The sun loses ~ 6.8×10^{16} Kg to the solar wind every year, this consider a very small amount of the sun's mass, as a continuous supersonic coronal expansion into the heliosphere, note that the solar wind shape the magnetosphere and the comets tails.

The solar wind plasma is an excellent thermal and electrical conductor, so the solar magnetic field intern the solar wind during expansion, by the rotation of the sun the magnetic field bent into spiral in the equatorial plane, the field lines make an angle ~45^0 with the radial direction at one Astronomical Unit (AU) as in Fig. (1.2)

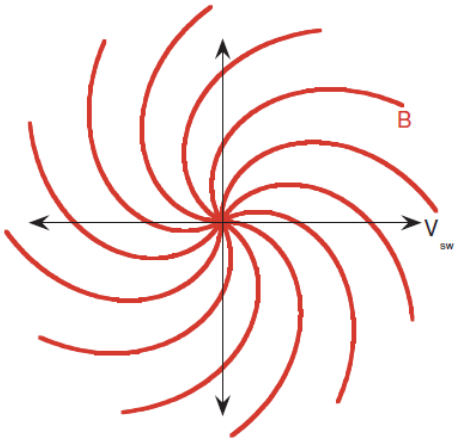

Figure 1.2 : configuration of the heliospheric magnetic field in the ecliptic plane for a uniform radial solar wind flow, [Lucy-Ann McFadden et al., 2007].

The solar wind is nonuniform and behaves as an alternating storms between high speed and low speed flow solar wind, the high speed solar wind reach 700 Km/s and generated from open magnetic field regions at the solar poles (latitude greater than 70^{o}), which called the coronal holes, while the velocity of low speed solar wind is around 400 Km/s, this component of solar wind originate from closed magnetic field region, at 1 AU the time between two collisions for a typical solar wind proton is several days, and the gyro radius for proton around 60 Km and for electron around 1.4 Km. The proton distribution function is anisotropic, (i.e. the proton parallel temperature is greater than perpendicular temperature), [Lucy-Ann McFadden et al., 2007].

The solar wind consists of protons in general (hydrogen ions) and electrons, The average abundance for elements in solar wind exhibit hydrogen dominant, the abundant of hydrogen relative to oxygen is 1900 times, the second is alpha particles which 75 times of oxygen, while the oxygen coming third, and there is a very small abundance of carbon, neon, nitrogen and other elements, [Lucy-Ann McFadden et al., 2007].

1.4 Earth's atmosphere and ionosphere layers

1.4.1. Atmosphere:

Our atmosphere stratified in horizontal layers due to gravity, studying and organizing these layers depends on temperature profile. The atmospheric temperature decreases with altitude from the surface up to 10 km, this layer called *troposphere* as shown in Fig. (1.3.a), and contains nearly 80% of the atmospheric mass, at higher altitudes the ozone absorption of extreme ultra violet EUV will increase temperature with altitude from 10 –

50 km, this layer called *stratosphere*, then the temperature start to decrease again by radiative cooling or CO_2 infrared cooling , decreasing in temperature continue for altitude around 90 km, this layer is called *mesosphere*, above mesopause (~ 90km) by absorption of UV and EUV radiation there is dramatically increasing of temperature at low altitudes of this layer (10-20 K/km), but at higher altitudes approaches a constant temperature, this layer is called *thermosphere,* it's sensitive layer to solar activity, [Michael C. Kelley et al., 2009].

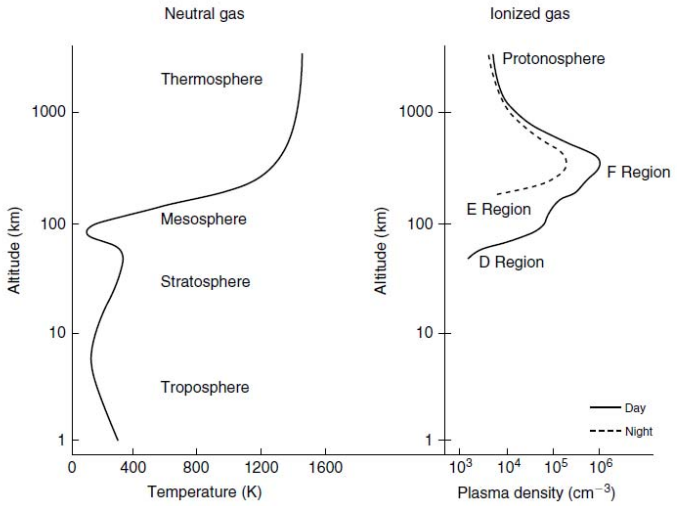

Fig. 1.3: typical profile for neutral atmospheric temperature at the left side, and the ionosphere plasma density at the right side, [Michael C. Kelley et al., 2009].

1.4.2. Ionosphere:

The ionization in thermosphere due to absorption of ultraviolet UV and EUV will change the neutral atmosphere to charged particles (plasma), so it's convenient to study the plasma ion density profile, or electron density, because electron density is semiequal of ion density. Hence, in space plasma physics is called *ionosphere*, and is divided into layers depending on plasma density profile as shown in Fig. (1.3,b).

The ionosphere is an interface between earth's atmosphere and the external space, above 85km ionization is dominant by ultraviolet solar radiation, and because the collisions are so rare then the recombination rate is slow, the ionization under 90 km is not excited, this region called D region, at this layer mainly O_2^+ and N_2^+ are produced. More ionization happen at altitude range 90-150 km, and is called E region. The main ionization process here is O_2^+ and NO^+ produced by (100-150 nm) UV radiation. The maximum density of

plasma occur at altitude in the range 150- 500 km and is called F region or F peak, mainly O^+ produced by (10-100 nm) UV light [Erik, 2009]. It is noted that different plasma densities between dayside and night side are shown in Fig. (1.3.b). Note the difference due to seasons, latitudes and solar cycle, because ions production is dependes on solar radiation.

1.5 Solar terrestrial interaction

1.5.1. The interaction:

There is an atmospheric escape of neutrals by thermal motion of atoms and molecules which energized by the solar UV heating. The most important process is the non-thermal escape of ions as plasma outflow along the open magnetic field lines at both poles.

The loss of matter due to outflow of protons from polar cap and aurora is in the order of 10^{26} ions/s [Cully et al.,2003; Huddleston et al., 2005], most of the polar wind outflow is H^+ ions because a negligible fraction of O^+ [Yau et al., 1988], however in the typical year loss matter due to outflow and accretion matter from interplanetary bodies are comparable.

The interaction of solar wind with the intrinsic magnetic field of earth lead to outflow of ionosphere plasma particles to magnetosphere. The solar wind expand in the interplanetary space and encounters the planets, moons and comets, our planet is one of them, since impact the earth's dipolar magnetic field forming asymmetric shaped magnetic cavity surrounding our planet. Solar wind compresses the magnetic field by the kinetic pressure on the dayside while the magnetic field at the nightside stretched out several hundreds to thousands of earth radii forming a *magnetotail*.

The earth's magnetic field make an obstacle for the supersonic solar wind flow, that is forming a *bow shock* (stands at average distances of 15 Earth radii (Re) at the sun earth line), the bow shock slows, heat and deflect the energized charged particles into *magnetosheath* region as shown in Fig. (1.4). The solar wind and the magnetosphere plasma cannot interpenetrate because the intrinsic magnetic field of the earth guides the charged particles, also because the embedded magnetic field of the solar wind which named as interplanetary magnetic field (IMF), this phenomena called frozen-in condition, frozen-in phenomenon mean that when highly conducting plasma approaches a magnetic field region, the magnetic field cannot penetrate into the plasma, that is applied on the magnetosphere and the solar wind, [Caroline Rayner et al., 2002].

The interaction between magnetosheath and terrestrial magnetosphere form a thin boundary layer between them called *magnetopause*, the magnetopause is an important layer in the solar-terrestrial physics, during reconnections this layer allow to exchange plasma and energy between vicinal regions, this layer occurs at the balance between solar wind and geomagnetic field pressures, and it's position expand and contract depending on solar wind strength, the magnetopause located in average at 11 Re towards the Sun on the sun earth plane. [Caroline Rayner et al., 2002].

The major interpenetrating place between solar wind and magnetosphere plasma is the north and south poles in the highly confined regions called the *polar cusp*s which take the funnel shape as shown in Fig. (1.4), the polar cusps provide a direct entry for solar wind charged particles, and the position of the cusps depend on IMF conditions, here the IMF connect with geomagnetic field and make like open geomagnetic field lines from the poles to interplanetary space (magnetotail).

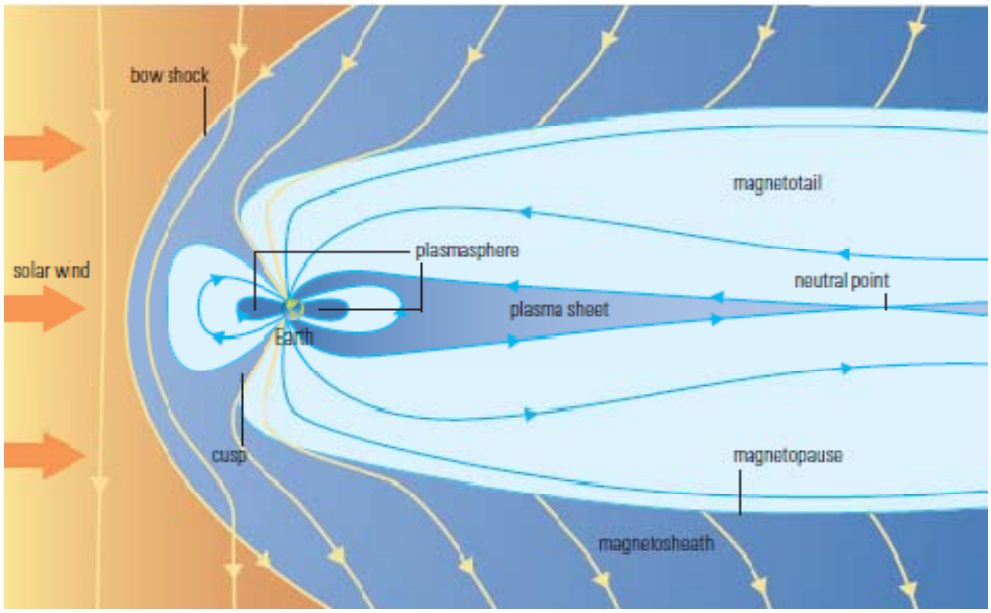

Figure 1.4 : Schematic illustration of the magnetosphere including important parts and boundaries like bow shock, magnetosheath, magnetopause, the cusps, plasmasphere, magnetotail. (Philips Astronomy Encyclopedia, 2002)

Open magnetic field lines permit light ions to escape away under the plasma pressure in ionosphere due to plasma density and temperature (ambipolar flow), the ion outflow occur at all latitudes but only at high latitudes ions escape directly to the outer magnetosphere along open magnetic field lines, This ion escape or out flow called the polar wind, it is important loss mechanism for ionosphere [Desseler and Michel, 1966; Axford, 1968].

At low latitudes ions will trapped within the closed magnetic field lines filling the plasmasphere. In the sunlit illuminations generate photoelectrons and given more acceleration for outflow at high altitudes and sweep the thermal ions with them [Tam et al., 1995; Su et al.,1998].

Plasma convection also affect the ionospheric outflow, because the solar wind is a magnetized plasma with high conductivity that impose an electric field as: $\boldsymbol{E} = -\boldsymbol{v} \times \boldsymbol{B}$, where E the electric field, v is the solar wind velocity and B is the magnetic field. This electric field across the polar cap , the plasma in open field lines will drift ($\boldsymbol{E} \times \boldsymbol{B}$) equatorward by the interaction between IMF and Earth's magnetic field , the plasma at low and middle latitudes corotate with the earth, but at high latitudes the solar wind-magnetosphere interaction produce electric field which rival the corotational electric field, then the result is convection pattern in the ionosphere [Schunk, 1999]. Convection in the cusp ion beams and conics into polar cap effect on the polar wind and make it unstable at high altitude and change the outflow rates [Barakat and Schunk , 1989; Chen and Ashour-Abdallah, 1990]. The convection time across the polar cap is comparable to polar wind flow from 1000-9000 km in altitude (Schunk and Sojka,1989,1997).

At high altitudes, more than $2R_e$, there is an electromagnetic wave turbulence which produce wave-particle interaction, and the result is perpendicular ion heating [Ludin et al., 1990; Barghouthi,1997], this factor is very important mechanism in ionospheric outflow in the aurora and polar cap, where our thesis scrutinize.

1.5.2. Aurora :

The aurora is an illumination of the sky at the night time in the upper atmosphere above 80 km (ionosphere), it is known as the northern and southern lights, the northern light is called aurora borealis and the southern one is called aurora australis [Barbier et al., 1950].

Some of the solar energetic particles can leak into magnetosphere along the open magnetic field lines or along the reconnection field lines at the magnetopause at the polar regions, the energized charged particles like electrons, protons, and heavier ions encounter and collide with atmospheric atoms at altitudes of 100 to 200 km, while these particles accelerated in the magnetosphere, this collisions caused dissociation of molecules to elements, ionization and excitation of atmospheric atoms and molecules, then the excited electrons back to stable state by emitting corresponding photon energy with discrete wave length, forming a sky colors called Aurora, [Michael C. Kelley et al., 2009].

Most of these colors are green and red which emitted at 557.7 and 630 nm wavelengths respectively, rays are due to excitation of upper oxygen atoms, while blue and other near ultraviolet emissions resulted from excitation of nitrogen molecules and ions. Aurora colors show gradient from green at the base (low altitude ~ 100 km) to red at the top of the illuminations ~ 150-600 km as shown in image (1.2) right part, this altitude depending color because oxygen has two ways to return to ground state, first by red emitting need long time comparative to green emitting, while the collisions prevent emissions by absorbing the oxygen excitation energy, so at high altitudes where the collisions are rare the red emissions have time to occur, but at lower altitudes green emission is dominant. The aurora lights may expand vertically for several hundred kilometers, and laterally for tens of degrees in longitude, where the base width is few kilometers in latitude, that show a narrow pattern of aurora display, like a waterfall of accelerated particles along a narrow field sheets to final depth of penetration, depositing their energy on the upper atmosphere, [Michael C. Kelley et al., 2009].

The Aurora encircle northern and southern geomagnetic poles, forming an oval shape which locate equatorward of the open geomagnetic field lines as shown in image (1.2) left side, the aurora located in average at 20^{o} from the pole at the day side, where at the night side 30^{o} from the pole. During the strong geomagnetic storms which related to sun's activities when the solar wind intensity increases by coronal mass ejections, the auroras are more frequent and the aurora ovals will be more brighten and will expands equatorward to be more broaden, and seen from lower latitudes, [Per Even Sandholt et al., 2004].

The aurora is not an exclusive on our planet, this phenomena is related with planets have a strong intrinsic magnetic field and an atmosphere, such as Jupiter, Saturn, Earth, Uranus, and Neptune, these planets have an auroral oval nearby the described above, while the weekly magnetized planets don't appears an auroral oval, like Venus and Mars.

Image 1.2 : the left photo depicts the Auroral oval (in false colour) as seen from space, overlaid on top of a visible image of Earth. The red indicates the brightest aurora and blue the dimmest. The brightest aurora is found at midnight. Copyright: Holzworth and Meng, NSSDC, NASA , 24 Aug 2006.

The right picture represent the aurora illuminations from the earth it shows the greened base and the altitude red extension, Copyright: Dave Ewoldt (Okarche, Oklahoma) , 13 November 2003.

1.5.3. Polar wind :

In analogy to solar wind, the coronal supersonic expansion, [Axford, 1968] coined the term "polar wind" to describe the polar supersonic outflow of thermal plasma. The polar wind is an ambipolar outflow of thermal plasma from the high-latitude ionosphere to the magnetosphere along "open" geomagnetic field lines. Another definition for the classical polar wind is the low density supersonic flux of cold light ions like H^+ and He^+ with some O^+ contributions through the polar cap into the magnetosphere associated with high solar activity [Schunk, 2000]. While the polar cap is the polar open magnetic field region surrounded by auroral oval.

The polar wind is an important source of magnetospheric plasma, in addition to some solar wind contribution, the polar wind is principal contributor of this plasma source, consist of electrons and light ions, by high abundance of hydrogen ions then helium ions with some contributions of oxygen ions.

The ion velocities are ranked inversely with the ion mass as $H^+ > He^+ > O^+$, For these species the bulk velocity is higher on the dayside than on the nightside, because the increasing of photoelectrons presence, that will create a large ambipolar electric field.

The outflow velocity increases with altitude to be supersonic at high altitudes, the O^+ outflow velocity starts to increase at altitude of about 5000 km, and reaches 1 km/s near 6000 km, and go around 4 km/s near the Akebono orbit (~10,000 km) [Abe et al., 1993].

The velocity of the polar wind ions is determined by a balance between various forces such as electric field, pressure gradient, gravity, and collisional force with other particles [Abe et al, 2004].

The polar wind outflow make transition between collision dominate region (barosphere) and collisionless dominate region (exosphere), separated by transition layer where the ions change their behavior from collision to collisionless dominant, also the transition occur from subsonic to supersonic ion velocities, and from heavy ions dominant to light ions dominant, and finally from chemical to diffusion dominance [Schunk, 1988].

The polar outflow rate is related with the solar activity and radiation, which can be measured by $F_{10.7}$ index, also related with the magnetic activity which measured by K_p index [Yau and Andre´, 1997], this reported dependences of the polar outflow with solar radiation and magnetic activity is clear for O^+ more than H^+, where the ionospheric heating will increase O^+ presence at high altitudes while the hydrogen neutral atoms will take enough kick to jump the gravity barrier decreasing the source of H^+. Because the mass difference between positive ions and the negative electrons separation distance in altitude by gravity is formed, making an ambipolar electric field due to partial charge separation allow heavy ions to accelerate upward enhancing the polar outflow. In addition to ambipolar electric field the pressure gradient also enhance the polar outflow, where the plasma pressure at ionosphere altitudes is greater than the plasma pressure at magnetosphere [Dessler and Michel, 1966; Axford, 1968]. The mirror force which also enhance the upward outflow at the polar regions due to the gradient in the magnetic field as will explain in the next chapter. Also the interaction between ions and the electromagnetic turbulence will increase the upward parallel outflow, this process called the wave particle interaction, the wave particle interaction is the main part of this thesis.

Chapter Two

Theoretical formulation

Chapter Two

Theoretical formulation

2.1 Plasma

Irving Langmuir who pioneered the study of ionized gases, and gave it the name, simply the plasma is quasi neutral ionized gas, which exhibit a collective behavior (like the ability of carrying electric field). By heating the matter change it's state from solid to liquid to gas, and the gases by heating transform to plasma (fourth state of matter) when atoms knock their electrons and then collisions between electrons and atoms liberate more electrons that produce positive charged ions and negative charged electrons which determine plasma characteristics. Electric and magnetic fields, the main specific for plasma that it is a high conductivity gaseous state and that is not found in natural conditions. The plasma is the main state of cosmic matter and plasma physics is very important in magnetic fusion energy researches, used by tokamaks, and important in astrophysics, like earth space plasmas such as the aurora, ionosphere, magnetosphere, polar wind, solar wind and the solar corona, [Bellan, 2004].

There is three fundamental parameters that characterize plasma: the particle density n(cm^{-3}), the temperature T of each species (eV), where 1 eV is equivalent to 11,605 K, and the steady state magnetic field B(Tesla). From these three fundamental parameters the subsidiary parameters can be derived like Debye length, Larmor radius, plasma frequency, cyclotron frequency and thermal velocity. High temperature of plasma not necessary means high of heating, because the density of plasma much less than density of gas in atmosphere pressure, heat capacity must be taken into account, $Q = m\, c\, \Delta T$, [Chen, 1984].

The plasma can have different temperatures at the same time, electrons and ions have a different Maxwellian distributions with different temperatures T_e and T_i , because the collision rate between the same species larger than collisions between different species in the plasma, even single species have two temperatures in absence of magnetic field, and two different Maxwellian distributions with temperatures $T_\perp$ and T_{II} , [Chen, 1984].

For the space plasmas the density vary from 10^6 m^{-3} like in the interstellar space, to 10^{20} m^{-3} like in the solar atmosphere, astrophysical plasmas that known have temperatures in the range of 1-100 eV and usually fully ionized.

2.2 Phase space and distribution function

Consider a particle moving in one dimension x and it's position and velocity varies with time, this motion can be presented in three dimensions *x* , *v* and *t* and this *x*-*v*-*t* space is called phase-space. In general the particle move in three dimensions, then we have *X*-*v*-*t* space where $\boldsymbol{X} = \boldsymbol{x} + \boldsymbol{y} + \boldsymbol{z}$ and $\boldsymbol{v} = \boldsymbol{v}_x + \boldsymbol{v}_y + \boldsymbol{v}_z$, this is a six dimensional space called phase space, and any point in phase space is represented by: $P=(x,y,z,v_x,v_y,v_z)$.

The function $f(\boldsymbol{X},\boldsymbol{v},t)$ which describes the instantaneous density of particles in phase-space is called the distribution function. The number of particles between *x* and *x*+*dx*, with velocities between *v* and *v*+*dv* could be change by their motion and acceleration under the effect of net force on them, then $f(x,v,t)$ will change.

Consider $f(x,v,t)$ the probability of randomly selected particle at position *x* with velocity *v* then averaging over the velocities of all particles at *x* gives the mean velocity *u(x)* determined by $n(x)\, u(x) = v\, f(x,v)\, dv$. In the same way we can give an expression for the mean energy of all the particles by multiplying $f(x,v)$ by v^2 and integrating over velocity multiplying $f(x,v)$ by various powers of *v* and integrating over velocity gives us moments of the distribution function. Then the density expression as: $n(x) = \int f(x,v)dv$ (2.1)

and the mean velocity becomes: [Bellan, 2004].

$$u(x) = \frac{\int v\, f(x,v)dv}{\int f(x,v)dv} \qquad (2.2)$$

2.3 Boltzmann Equation

Rate of change of the distribution function under many external forces and collisions can be described by Boltzmann equation which describes each species in separate distribution function [Bellan, 2004], Boltzmann equation is :

$$\frac{\partial f}{\partial t} + \boldsymbol{v}.\nabla f + \boldsymbol{a}.\nabla_v f = \frac{\delta f}{\delta t} \qquad (2.3)$$

Where $f = f(r,v,t)$, $\nabla = \frac{\partial}{\partial x}\mathrm{i} + \frac{\partial}{\partial y}\mathrm{j} + \frac{\partial}{\partial z}\mathrm{k}$ (space gradient)

$$\nabla_v = \frac{\partial}{\partial v_x}\mathrm{i} + \frac{\partial}{\partial v_y}\mathrm{j} + \frac{\partial}{\partial v_z}\mathrm{k} \text{ (velocity space gradient)}$$

where the acceleration of the particle due to Lorentz force and gravity is:

$$\boldsymbol{a} = \boldsymbol{g} + \frac{q}{m}[\boldsymbol{E} + \boldsymbol{v} \times \boldsymbol{B}] \qquad (2.4)$$

The first term on the left side of eq 2.3 represents the change of f for species at fixed point in space, while the second term represent the change of f for species move in velocity (v) in space, and the third term represent the change of f for **species** accelerating in velocity space, and the right hand side represent the rate of change of f in a given region of phase space due to collisions. Where g is gravitational acceleration , q and m are the charge and mass of the species, E and B are electric and magnetic fields, [Bellan, 2004].

Boltzmann equation will be used in the present study in polar out flow region at high latitude and altitude, where the collision is neglected, the effect of gravity and polarization electric field and geomagnetic field are strongly present in addition to wave particle interaction which will be explained in details later.

2.4 Charged particles in a magnetic field

The plasma sometimes behave like fluids, and sometimes as a collection of individual particles, so it's important to understand the behavior of single particle in electric and magnetic fields. As known, when the charged particle move with velocity $\boldsymbol{v}$ in the presence of magnetic field **B,** and absence of the electric field (**E**=0) Lorentz force will be:

$$\boldsymbol{F}_{mag} = q(\boldsymbol{v} \times \boldsymbol{B}) \qquad (2.5)$$

The charged particles will move in circular motion as in figure(2.1), in this case the charged particles has simple cyclotron gyration, from *cyclotron formula* we can get the radius of the circle which called Larmor radius (gyro radius)

$$r_L = \frac{v_\perp}{\omega_c} = \frac{mv_\perp}{qB} \qquad (2.6)$$

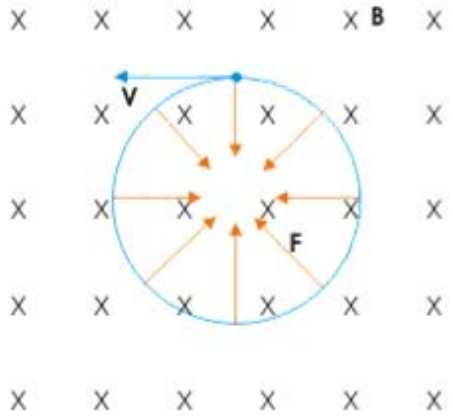

Figure (2.1): Motions of a charged particle in magnetic field
http://cnx.org/content/m31345/latest/ (2011)

It is assumed that the particle moves in perpendicular plane to **B**, but in general the particle has two velocity components parallel and perpendicular($v_\parallel$, $v_\perp$) to **B** and the particle will move in helix with the same Larmor radius as in figure (2.2).

From the equation of motion, the Larmor frequency (gyro frequency) is follows:

$$\omega_c = \frac{qB}{m} \qquad (2.7)$$

Note that Larmor frequency and the time period of revolution are independent of the speed of the particle, which is an important result to be used in cyclotron.

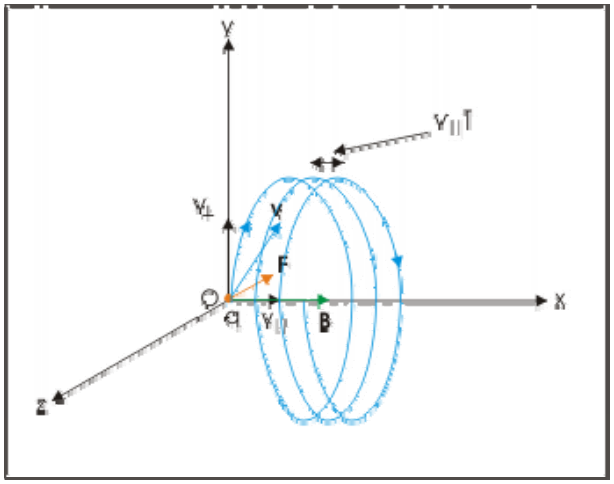

Figure (2.2) : Helical path motion of charged particle in uniform magnetic field http://cnx.org/content/m31345/latest/ (2011)

The magnetic force change in the particle direction (the direction of $v_{\perp}$) but cannot change the particle speed (the magnitude of $v_{\perp}$ or $v_{\parallel}$) because the magnetic force perpendicular on the particle motion and do no work, in other words the perpendicular velocity component results a centripetal force moving the particle in circular path, but the parallel velocity component results zero magnetic force then the motion in this direction without acceleration, the result is helixal motion of the charged particle and the gyration of electron or ion be parallel or anti parallel to the magnetic field lines.

The ratio of charge and mass of the particle $\frac{q}{m}$ is known as specific charge it has special importance in describing motion of charged particle in magnetic field. The magnetic force is proportional to charge q, where the acceleration of the charged particle inversely proportional to mass m.

If the magnetic field has strong gradient as the magnetic bottle shown in figure 2.3, the ion will be reflected, this is known as ion mirror or mirror force. The particle gyrates around and travels right or left along the field line, just as in a uniform field. The angle between the velocity vector of the particle and the magnetic field direction at any point is called the pitch angle [Gosling et al., 1973], when the particle approaches stronger magnetic field, its spiral motion tightens up, and the pitch angle increases, when the pitch angle reachs 90 degrees the

particle gyrates only around the field line but not along it. The particle then starts to turns toward the other mirror point in the other side which called the mirror force.

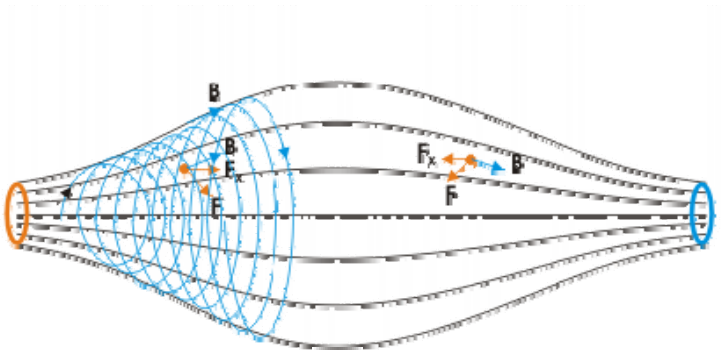

Figure (2.3): Charged particle trap in strong gradient magnetic field
http://cnx.org/content/m31345/latest/ (2011)

The charged particles near the earth follow the same behavior, because the magnetic field is not uniform, (i.e. stronger at high latitude in both hemispheres).

2.5 Polarized electrostatic field

By the geomagnetic field the charged particles, i.e. electrons and ions will move along the field lines, there is a clear difference of mass between them so the gravity leave electrons arise more than the heavy ions, that make a slight charge separation forming polarized electrostatic field, electrons then moving due to temperature and density gradient and gravity. To describe the plasma outflow after many approximation like diffusion approximation were done to reach the momentum equation for electrons [Schunk and Nagy,2000].

$$\nabla_{\parallel} p_e + (\nabla . \boldsymbol{t}_e)_{\parallel} + n_e e E_{\parallel} - n_e m_e g_{\parallel} = n_e m_e \nu_{ei}(u_i - u_e) + n_e m_e \nu_{en}(u_n - u_e)_{\parallel} \quad (2.8)$$

Where p_e is the electron partial pressure , $E_{\parallel}$ is the polarization electrostatic field, n_e electron density, m_e electron mass, $g_{\parallel}$ parallel component of gravity acceleration with magnetic field line, $\mathbf{t}_e$ electron stress tensor, ν collision frequency, and u the drift velocity. By approximation, for simplicity the mass of electron m_e can be neglected in eq (2.8). Therefore, by dropping out all terms contain electron mass, to get :

$$n_e e E_{\parallel} = -\nabla_{\parallel} p_e \qquad (2.9)$$

For isothermal electron gas , and letting $E_{\parallel} = -\nabla_{\parallel} V_p$, where V_p is the polarization potential (due to polarization electric field), and $p_e = n_e k T_e$,and assume T_e is constant , from equation (2.8) we get :

$$\frac{e}{kT_e}\frac{\partial}{\partial r}V_p = \frac{1}{n_e}\frac{\partial}{\partial r}n_e \qquad (2.10)$$

Where, r is the spatial coordinate either along or perpendicular to geomagnetic field lines, by integration Boltzmann equation is obtained:

$$n_e = n_0 e^{\frac{eV_p}{kT_e}} \qquad (2.11)$$

Where n_0 is the equilibrium electron density at V_p=0 .

Now by taking the natural logarithm of both sides and then take the exponential to get the potential energy due to the polarization electric field, [Barghouthi, 2008]:

$$\phi_p = e\, V_p = kT_e ln\left[\frac{n_e}{n_0}\right] \qquad (2.12)$$

2.6 Gravitational force :

Any two bodies or two particles in the universe are attractive by Newtonian gravity attractive force which indirect proportional with thier masses and inversely proportional with the distance between them, the ions and our planet are also affected by this force :

$$\boldsymbol{F}(r) = \frac{G\, M\, m}{r^2}\, \hat{r} \qquad (2.13)$$

Where G is a universal gravitational constant , M is the mass of earth ,m is the ion mass , r is the distance between the ion and the earth and r̂ is a unit vector. From the work done by the force:

$$W = -\Delta\phi(r) = -\int_{r_0}^{r} F(r).\, dr \qquad (2.14)$$

Where $\phi(r)$ is the gravitational potential energy , and r_0 is the lower boundary geocentric distance of our simulation tube and equal 1.7Re ,and r the geocentric distance which represent the location of the ion. Substituting equation 2.13 in equation 2.14 to get:

By substitution of eq 2.3 in eq 2.4 we have:

$$\Delta\phi(r) = -GMm\int_{r_0}^{r}\frac{dr}{r^2} = GMm\left[\frac{1}{r_0}-\frac{1}{r}\right] \qquad (2.15)$$

Then the final potential energy is the summation of gravity term and polarization electric field term, which is given by [Barakat and Schunk, 1983] as:

$$\phi_p = e\,V_p = kT_e \ln\left[\frac{n_e}{n_0}\right] + GMm\left[\frac{1}{r_0}-\frac{1}{r}\right] \qquad (2.16)$$

2.7 Wave particle interaction (WPI)

The interaction between ions and electrostatic or electromagnetic waves evolve energy transfer from the waves to the ions and energize the ion conics by the essentially perpendicular component of electric fields [Skiff et al., 2000].

Wave particle interaction is the model which will be used in our study for studying the outflow of the ions from ionosphere to magnetosphere in the polar cap region. Several models were used to investigate the behavior of plasma outflow, centrifugal acceleration, enhanced ion and electron temperature, strong ionosphere convection, external ion heating, and wave particle interaction [Yau et al., 2007]. The main idea in wave particle interaction that the electromagnetic turbulences affect the ion velocity distribution by the heating in perpendicular direction to the magnetic field lines increases the upward force due to converging of magnetic field lines which called mirror force.

Wave-particle interaction of ions with plasma turbulence at high latitudes of the earth accelerate this ions [Barghouthi et al, 2007]. The effect of wave-particle interactions on ion outflows in the polar wind and aurora region is very important to investigate, because the escape of the ionospheric ions to the magnetosphere is an important ionosphere-magnetosphere coupling mechanism.

The effect of wave-particle interactions is represented by particle diffusion in the velocity space [Retterer et al.,1987a]:

$$\left(\frac{\partial f}{\partial t}\right)_{WPI} = \frac{1}{v_\perp}\frac{\partial}{\partial v_\perp}\left(D_\perp v_\perp \frac{\partial f}{\partial v_\perp}\right) \qquad (2.17)$$

where $D_\perp$ is the quasi-linear velocity diffusion rate perpendicular to geomagnetic field lines.
By some assumption for simplicity [Retterer et al, 1987b] found that :

$$D_\perp = \frac{\eta q^2}{4m^2}\,|E_x(\omega = \Omega)|^2 \qquad (2.18)$$

Where q is the ion charge, m is the ion mass, Ω is the ion gyrofrequency, ω is the angular frequency of the electromagnetic turbulence, $|E|^2$ is the spectral density of the wave, and η is the proportion of this density that corresponds to left hand polarized wave.
The velocity diffusion rate $D_\perp$ given in eq (2.18) is velocity and altitude independent, it depends on the altitude through the variation of the ion gyrofrequency Ω, along the geomagnetic field lines. [Barghouthi,1997; and Barghouthi et al., 1998] improved $D_\perp$altitude dependence, processed the data collected by Plasma Wave Instrument PWI on board the DE-1 spacecraft. The result is the following expressions for altitude dependent velocity diffusion coefficient $D_\perp$ in the region equatorward of the cusp:

$$D_\perp(r) = \begin{cases} 5.77 \times 10^3 (\frac{r}{R_E})^{7.95} cm^2 sec^{-3}\,, & for\ H^+ \\ 9.55 \times 10^2 (\frac{r}{R_E})^{13.3} cm^2 sec^{-3}\,, & for\ O^+ \end{cases} \qquad (2.19)$$

But this expression did not explain the non-Maxwellian features of H^+ and O^+ at mid and high altitudes, the correction for this expression suggested by [Retterer et al.,1994] , that requires a velocity dependent diffusion rate .
There are three models (velocity dependent diffusion coefficient expressions), which will be discussed in detail.

2.7.1 Barghouthi model :

The geomagnetic field intensity will decrease with altitude, inversely proportional, $B \sim r^{-3}$, then the gyration radius (r_L) of the ion will increase. At high altitudes the gyration radius will increase and become comparable with $\lambda_\perp$ (perpendicular electromagnetic turbulence wavelength), then the value of ($\frac{k_\perp v_\perp}{\Omega}$) become greater than one, since [Barghouthi, 1997 and Barghouthi et al,1998] develop altitude and velocity dependent diffusion coefficient for these altitudes. As shown in the following equation (2.20):

$$D_\perp(r, v_\perp) = \begin{cases} \begin{cases} 5.77 \times 10^3 (\frac{r}{R_E})^{7.95} cm^2 sec^{-3}, & for\ H^+ \\ 9.55 \times 10^2 (\frac{r}{R_E})^{13.3} cm^2 sec^{-3}, & for\ O^+ \end{cases} & for \quad \left(\frac{k_\perp v_\perp}{\Omega}\right) < 1 \\ \begin{cases} 5.77 \times 10^3 (\frac{r}{R_E})^{7.95} \left(\frac{k_\perp v_\perp}{\Omega}\right)^{-3} cm^2 sec^{-3}, & for\ H^+ \\ 9.55 \times 10^2 (\frac{r}{R_E})^{13.3} \left(\frac{k_\perp v_\perp}{\Omega}\right)^{-3} cm^2 sec^{-3}, & for\ O^+ \end{cases} & for \quad \left(\frac{k_\perp v_\perp}{\Omega}\right) \geq 1 \end{cases}$$

---------- (2.20)

2.7.2 RCC model :

In 1985 Crew and Chang used the frequency spectrum observations suggest the velocity dependence of velocity diffusion coefficient in this form:

$$D_\perp(v_\perp)\ \alpha\ \left(\frac{v_\perp}{v_o}\right)^\beta \left(1 + \left(\frac{v_\perp}{v_o}\right)^{\beta+1}\right)^{-1} \qquad (2.21)$$

where v_o is the reference phase velocity, β is a parameter dependant on the shape of the spectrum curve and chosen to be unity by [Chang, 1993]. [Barghouthi, 2008] suggest a model for the diffusion coefficient $D_\perp$ as a function of perpendicular velocity, and the position along the geomagnetic field lines based on the work of [Barghouthi et al., 1998] then the above perpendicular diffusion coefficients, $D_\perp$ (O^+) and $D_\perp$ (H^+) will be given as a function of velocity and altitude in the polar cap region as follows:

$$D_{\perp}(H^{+}) = 5.77 \times 10^{3} \left(\frac{r}{R_E}\right)^{7.95} \left(\frac{v_{\perp}}{v_0}\right) \left[1 + \left(\frac{v_{\perp}}{v_0}\right)^{4}\right]^{-1}$$

$$D_{\perp}(O^{+}) = 9.55 \times 10^{2} \left(\frac{r}{R_E}\right)^{13.3} \left(\frac{v_{\perp}}{v_0}\right) \left[1 + \left(\frac{v_{\perp}}{v_0}\right)^{4}\right]^{-1} \qquad (2.22)$$

The value of v_0 is the ion thermal velocity at the lower boundary. These altitude and velocity dependent diffusion coefficients will be used to investigate the effects of altitude and velocity dependent WPI on the outflow of H^+ and O^+ ions in the polar cap region.

2.7.3 Bouhram model :

Velocity dependent diffusion coefficient also found by [Bouhram et al., 2004] as :

$$D_{\perp} \alpha\, J_0^2(k_{\perp 0}\rho) = J_0^2\left(\frac{k_{\perp 0} v_{\perp}}{\omega_c}\right) = J_0^2\left(\frac{2\pi v_{\perp}}{\lambda_{\perp 0}\omega_c}\right) \qquad (2.23)$$

Where J_0 is the zeroth order of standard Bessel, $k_{\perp}$ is the perpendicular component of the wave vector k, and ω_c is the ion gyrofrequency, note that $\rho = v_{\perp}/\omega_c$ denotes the ion gyroradius. Now there is a velocity dependent diffusion coefficient, but need to take the position along the geomagnetic field also in the simulation, so it is convenient to add the above conclusion to [Barghouthi, 1997] altitude dependence to have :

$$D_{\perp}(r) = \begin{cases} 5.77 \times 10^{3} \left(\frac{r}{R_E}\right)^{7.95} J_0^2\left(\frac{2\pi v_{\perp}}{\lambda_{\perp 0}\omega_c}\right) cm^2 sec^{-3}, & for\ H^{+} \\ 9.55 \times 10^{2} \left(\frac{r}{R_E}\right)^{13.3} J_0^2\left(\frac{2\pi v_{\perp}}{\lambda_{\perp 0}\omega_c}\right) cm^2 sec^{-3}, & for\ O^{+} \end{cases} \qquad (2.24)$$

This form will be a velocity and altitude diffusion coefficient for Bouhram model to investigate ion outflow from ionosphere to magnetosphere in polar cap region.

2.8 Monte Carlo Simulation MC :

2.8.1 Monte Carlo Method and Boltzmann equation

Computer simulation is very important in physical science, specially plasma physics, computer simulation allows to improve theories (models). Plasma medium consist of electrons, ions and neutral atoms, and there motion under many external effects like geomagnetic field, polarization electric field, gravity and internal interactions between them is difficult to calculate and understand, so Monte Carlo method is a powerful technique to simulate plasma, Monte Carlo depends on random numbers and probability statistics, this technique deal with plasma by separate velocity distribution function for each species, and describe the motion of minor ion in a major background of ions, the change of velocity distribution function can be describe by Boltzmann equation , so to get the distribution function for the ion and it's moments, Boltzmann equation must be solved by more success methods like Monte Carlo method, Boltzmann equation [Schunk,1977] :

$$\frac{\partial f}{\partial t} + \boldsymbol{v}.\nabla f + \frac{q}{m}(\boldsymbol{E} + \boldsymbol{v} \times \boldsymbol{B}).\nabla_v f = \frac{\delta f}{\delta t} \qquad (2.25)$$

Where **E** is the electric field, **B** is the magnetic field, $\boldsymbol{v}$ is the velocity of the particle, q is the species particle charge, m is the species particle mass and $\frac{\delta f}{\delta t}$ represent the change in distribution function due to collisions. So we will use Monte Carlo simulation to solve Boltzmann equation to find the velocity distribution for H^+ and it's moments like density, drift velocity, parallel temperature and perpendicular temperature [Barghouthi et al., 2003b].

The simulation tactics is to follow the ion's motion for large number of collisions, first from boundary condition and from known velocity distribution function the ion is injected with randomly initial velocity (taken from ion's distribution function), by proper random number generator get the time interval between two collisions, during this interval the ion's trajectory determined by classical laws of motion of charged particle under many effects which mentioned above, according to chosen collision model the change of velocity of the ion due to collisions determined by using statistical properties represented by another random number [Barghouthi, 1997;Barghouthi et al., 1998].

$$f\ v\ = n\left(\frac{}{2\pi kT}\right)^{-} e \qquad {}^{2}_{\parallel}+v_{\perp}^{2})/2kT \qquad (2.26)$$

Where n is the number density, m is the ion's mass, k is the Boltzmann constant, T is the ion temperature, where v is the random ion's velocity, we substitute v^2 as $(v_{\parallel}^2 + v_{\perp}^2)$ because the ion's velocity has parallel and perpendicular components with respect to the magnetic field direction.

So we can write the velocity distribution function as :

$$f(v) = n\, f(v_{\parallel}) f(v_{\perp}) \qquad (2.27)$$

Where $f(v_{\parallel})$ is the parallel velocity distribution function and $f(v_{\perp})$ is the perpendicular velocity distribution function [Barakat et al., 1994].

note $\quad f(v_{\parallel}) = \left(\frac{m}{2\pi kT}\right)^{\frac{1}{2}} e^{-mv_{\parallel}^2/2kT}$, $\quad f(v_{\perp}) = \left(\frac{m}{2\pi kT}\right) e^{-mv_{\perp}^2/2kT}$ (2.28)

The above distribution functions will be used to generate random injected ion's perpendicular and parallel velocities.

2.8.2.1 Perpendicular velocity generation

At the injected point the random value for perpendicular velocity at the interval (0,∞) can be found by [Aldrich, 1985]:

$$\int_0^{v_{\perp}} p(v_{\perp}^{'}) dv_{\perp}^{'} = G \qquad (2.29)$$

Where $p(v_{\perp}) = 2\pi v_{\perp} f(v_{\perp})$, $p(v_{\perp})$ is the probability density , and G is a random number between 0 and 1, so we can get the value of $v_{\perp}$ of the randomly injected ion by solving the above equation as the following:

$$v_{\perp}^2 = -\left(\frac{2kT}{m}\right) \ln(1 - G) \qquad (2.30)$$

2.8.2.2 Parallel velocity generation

The difference between the number of ions with $v_{\parallel}$ and the number of ions pass the lower boundary of simulation region must be recognized, if the ion has $v_{\parallel} < 0$ then the ion will not cross the lower boundary, and the ions which can cross the assumed injected boundary must have $v_{\parallel} > 0$,the probability density of ions which cross the lower boundary is given as:

$$p(v_{\parallel}) = 2\pi v_{\parallel} \left[\frac{m}{2\pi kT}\right] e^{-mv_{\parallel}^2/2kT} \qquad (2.31)$$

So the parallel velocity of the passed ions is given by:

$$v_{\parallel}^2 = -\left(\frac{2kT}{m}\right)\ln(1-G) \qquad (2.32)$$

There is similarity for formula of parallel and perpendicular velocities, but different numerical values because of G, because we here generate an ion randomly from Maxwellian distribution at the boundary level.

2.8.3 Distribution function and it's moments:

Large number of injected test ions was used to the simulation region, velocity grid used in velocity space consist of bins, the bin's volume in velocity space is $\Delta^3 v = 2\pi v_{\perp}\Delta v_{\parallel}\Delta v_{\perp}$. The time needed to cross the bin is $t = c_1/|v_{\parallel}|$, where c_1 is arbitrary constant.

The time that an ion spends in each bin is divided by the bin's volume and is taken to be proportional to the ion's velocity distribution function at it's center [Barghouthi, 1997; Barghouthi et al.,1998].

The result is the following:

$$f(v) = \frac{c_2/|v_{\parallel}|}{2\pi v_{\perp}\Delta v_{\parallel}\Delta v_{\perp}} \qquad (2.33)$$

Consider the width of each bin is 1/3 of the thermal speed of the background ions, as $\frac{1}{3}\left(\frac{2Kt}{m}\right)^{\frac{1}{2}}$ which equal $\Delta v_{\parallel}$ and $\Delta v_{\perp}$, by knowing the parallel and perpendicular velocities it is possible to determine the bin, mean the location of the test ion, then input of the numerical value of $f(v)$ at the bin and add the numerical value of $f(v)$ for any other test ion located at that bin.

The low order of moments (i.e. density, drift velocity, parallel temperature and perpendicular temperature), the definitions of the velocity moments as the following:

The Density

$$n_s = \int f_s\,(v_s) d^3 v_s \qquad (2.34)$$

Drift velocity

The drift velocity u of the test ions is equal to the expectation value of $v_{\|}$.

$$u_s = \frac{\int v_{\|} f(v_s) d^3 v}{\int f(v)\, d^3 v} \qquad (2.35)$$

Perpendicular and parallel temperature

The random thermal velocity is defined as c = v – u . The expectation value for the kinetic energy ($\frac{1}{2}mc^2$) equal thermal energy $\frac{3}{2}kT$.

$$\frac{1}{2}kT_{\|} + kT_{\perp} = \frac{\int \frac{1}{2} m(v_{\|} - u)^2 f(v) d^3 v}{\int f(v) d^3 v} + \frac{\int \frac{1}{2} m {v_{\perp}}^2 f(v) d^3 v}{\int f(v) d^3 v} \qquad (2.36)$$

Then the parallel temperature is defined as

$$T_{\|} = \frac{m \int (v_{\|} - u)^2 f(v) d^3 v}{k \int f(v) d^3 v} \qquad (2.37)$$

And the perpendicular temperature is defined as

$$T_{\perp} = \frac{m \int {v_{\perp}}^2 f(v) d^3 v}{2k \int f(v) d^3 v} \qquad (2.38)$$

Chapter Three

The Results

Chapter three

The results

3.1: Introduction:

This results to understand the plasma ions behavior at high altitudes and latitudes under the effect of forces of gravity, polarization electric field, geomagnetic field, and the effect of electromagnetic turbulences which called wave particle interaction. Computer simulation was used based on Monte Carlo Method, which explained in the previous chapter. There is three theoretical models in our simulation, these three models are the most successful in prediction comparison with observations, these models are Barghouthi, Bouhram and RCC, models.

The large area of the polar cap makes it a significant source of ions via the relatively low energy ion outflow known as the polar wind [Barghouthi, 1997]. The polar wind is our region to investigate the behavior of H^+ ions which form a major ion in the polar wind.

The simulation starts from 1.7 Re altitude to 13.7 Re as a simulation tube, and use the following boundary condition at lower boundaries (1.7 Re), the temperature of H^+ ions is 3000 K, the H^+ ion density is 200 /cm^3 ,the drift velocity is 11 km/s, these boundary conditions are a probe or satellite observations, the distribution function at the boundary assumed to be Maxwellian, the electromagnetic wave length is 8 km according to [Barghouthi, 2008], where the electron temperature assumed to be constant at 1000 K, the simulation choose randomly an initial ion velocity corresponding to ion distribution function at the boundary, the test ion move for short interval of time Δt under the effect of gravity, divergence geomagnetic field and electrostatic polarization, this region considered to be collisionless, and the geomagnetic field intensity is proportion inversely with the geocentric distance as $B\ \alpha\ \frac{1}{r^3}$, and the ion behavior is controlled by the conservation of the energy and the first adiabatic invariant μ. The effect of the WPI during the simulation period Δt participate in calculation as a perpendicular perturbation on the ion velocity by random increment $\Delta v_\perp$ such that:

$$\langle (\Delta v_\perp)^2 \rangle = 4 D_\perp (r, v_\perp) \Delta t$$

This condition is common for our three models, Barghouthi model, RCC model, and Bouhram model. First model presented is RCC, presents altitude dependant $D_\perp(r)$ and velocity dependant $D_\perp(r, v)$ to distinguish the effect of velocity in wave particle interaction.

3.2: RCC model:

RCC model explained in section 2.7.2 , two steps were used for results production according to this model in the polar wind region, the first is simulation with altitude dependant $D_{\perp}$, that mean no velocity dependence, and then obtain the simulation for velocity and altitude dependent wave particle interaction.

The results are shown in Fig (3.1), output results for 14 different altitudes from 1.7 Re to 13.7 Re to show the changes for H^+ ion distribution function $f(H^+)$, we have two different columns the left for altitude dependent $D_{\perp}$ and the right for velocity and altitude dependant $D_{\perp}$. These two columns allow comparison between them for better understanding to the effect of velocity in the wave particle interaction and perpendicular ion heating process.

At the injection point, 1.7 Re, the randomly injected velocity distribution is corresponding to the boundary conditions which mentioned previous page, at the exobase the Maxwelian distribution function for both cases altitude dependent and velocity-altitude dependent, the behavior of distribution function for both cases is identical up to 4.2 Re , where the effect of velocity dependence of $D_{\perp}$ is negligible, it's effect emerge at 5.2 Re and starts to make difference between the two cases as altitude increases, at the velocity dependant (right hand columns), the anisotropy is dominant in the range between 5.2Re to 7.6 Re as shown in figure 3.1, where $T_{\parallel}(H^+) > T_{\perp}(H^+)$ due to adiabatic cooling and weakness of wave particle interaction at this altitudes, because Larmor radius is small compared with the electromagnetic wavelength, at 8.1 Re WPI starts to balance, while at 9.3 Re the WPI exceed the adiabatic cooling and the perpendicular velocity will increase with altitude forming the conic shape which related to wave particle interaction that heats the ion in perpendicular direction [Barghouthi, 2008], because the gyro radius approaches the electromagnetic wavelength, at 11.9 Re developing of toroidal shape is very clear, then complete at 13.7 Re, this shape is dominant and saturate at very high altitudes .

The toroidal shape can be explained by the peaked nature of velocity diffusion rate coefficient ($D_{\perp}$) , here we used the expression of RCC in equation 2.22 for hydrogen ion, where the perpendicular velocity $v_{\perp}$ is small then the $D_{\perp}(H^+)$ also will be small, and when the value of the perpendicular velocity increases and approaches v_0 the value of diffusion coefficient will be valuable, and wave particle interaction process will be dominant .

When the value of $v_\perp$ increases to great values the diffusion coefficient will decrease as $\left(\frac{v_\perp}{v_0}\right)^{-3}$ so the limitation for WPI will produce saturation in the toroidal shape at higher altitudes, then the ions tend to move out of large $D_\perp$ regions to low $D_\perp$ regions (high perpendicular ion velocity), that form the famous contour shape for velocity distribution function which called toroidal shape (Donuts), the toroidal shape of the velocity distribution saturates because the effect of perpendicular heating becomes negligible [Barghouthi, 2008], while in altitude dependent (the left columns in Fig (3.2)) the toroidal features didn't appear in results, we just detect a conic shape dominant above 8.1 Re , then this feature saturate to highest altitudes, that under effect of only altitude dependant velocity diffusion coefficient $D_\perp$.

Figure 3.1 : the velocity distribution function of H^+ ions in the polar region according to RCC model, we introduce 14 different altitudes from 1.7 Re geocentric distance to 13.7 Re, the electromagnetic wavelength ($\lambda_\perp$) used equal 8 km , the distribution function for H^+ ions represented by equal values contours in the normalized velocity plane ($c_\parallel$, $c_\perp$), where $c = \frac{[v - u(H^+)]}{[\frac{2kT(H^+)}{m(H^+)}]^{1/2}}$. (next page)

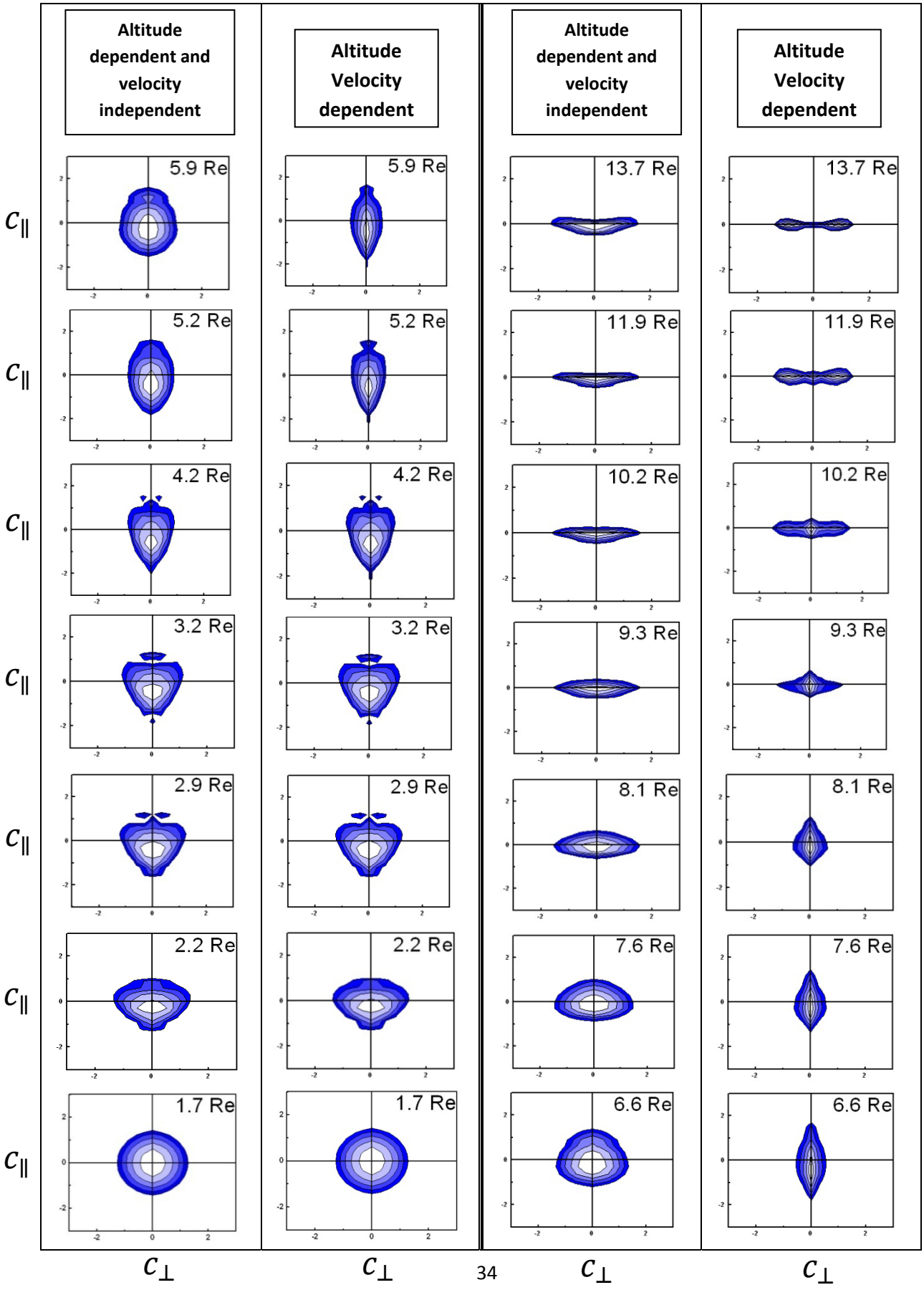
Altitude dependent and velocity independent
Altitude Velocity dependent
Altitude dependent and velocity independent
Altitude Velocity dependent
5.9 Re
5.9 Re
13.7 Re
13.7 Re
5.2 Re
5.2 Re
11.9 Re
11.9 Re
4.2 Re
4.2 Re
10.2 Re
10.2 Re
3.2 Re
3.2 Re
9.3 Re
9.3 Re
2.9 Re
2.9 Re
8.1 Re
8.1 Re
2.2 Re
2.2 Re
7.6 Re
7.6 Re
1.7 Re
1.7 Re
6.6 Re
6.6 Re
$c_{\parallel}$
$c_{\perp}$

To understand the ions behavior under many forces as mentioned before, it is important to study the lower order moments of hydrogen ions inserted in Fig (3.2), the altitude profile is shown for density $n(H^+)$, drift velocity $u(H^+)$, perpendicular temperature $T_\perp$ and the parallel temperature $T_\parallel$, altitude and velocity dependent WPI was plotted in black solid line, and the altitude dependent WPI (velocity independent) in red solid line.

At the top right of Fig (3.2) the drift velocity altitude profile show an increases in velocity with altitude, the velocity dependent WPI (black one) exhibit limitation for increasing of velocity compared with velocity independent curve, the reduction of particles acceleration occur by the reduction of $D_\perp$ at highest altitudes due to increasing of the perpendicular velocity, this process emerge at high altitude above 7 Re. The net flux is constant so the limitation of increasing the velocity at higher altitudes balanced by increasing of H^+ ion density at these altitudes, note that in density panel at the top left, where the density in velocity dependant curve (black one) more than the density in velocity independent (red line) above 8 Re.

The competitor of wave particle interaction is the perpendicular adiabatic cooling, where the perpendicular heating process due to WPI is faced by perpendicular adiabatic cooling, that is very crucial in perpendicular temperature profile (left bottom), it's clear that the adiabatic cooling dominate at low altitudes up to 4 Re, where the perpendicular temperature decreases with altitude, then above this altitude the WPI effect start to inverse the process by the perpendicular heating, so $T_\perp$ will increases with altitude, this behavior will dominate to high altitudes then tend to saturate at 11 Re, if we compare between velocity dependant (black) and independent (red), we can note that the effect of velocity dependant WPI will limit the increasing of perpendicular heating which overstated in velocity independent curve (the red).

The parallel temperature of hydrogen ions $T_\parallel(H^+)$, presented in Fig (3.2) in the down right panel, the altitude profile for $T_\parallel(H^+)$ give a clear correlation between perpendicular and parallel temperatures, the adiabatic cooling gives an abrupt dominate at lower altitude then start to straighten at higher altitudes by the effect of WPI, then the behavior of parallel temperature profile depend on perpendicular heating and adiabatic cooling, and the energy transfer from perpendicular to parallel direction by the ion drifting along diverging magnetic field which increases the parallel temperature, the velocity dependent WPI (black) retard the energy transformation from perpendicular to parallel direction, so arrest the increasing of $T_\parallel$.

In the velocity dependant (black curve) the parallel temperature decreases very slowly with altitude, while in perpendicular temperature (left bottom) which decreases very rapidly in order to conserve the first adiabatic invariant.

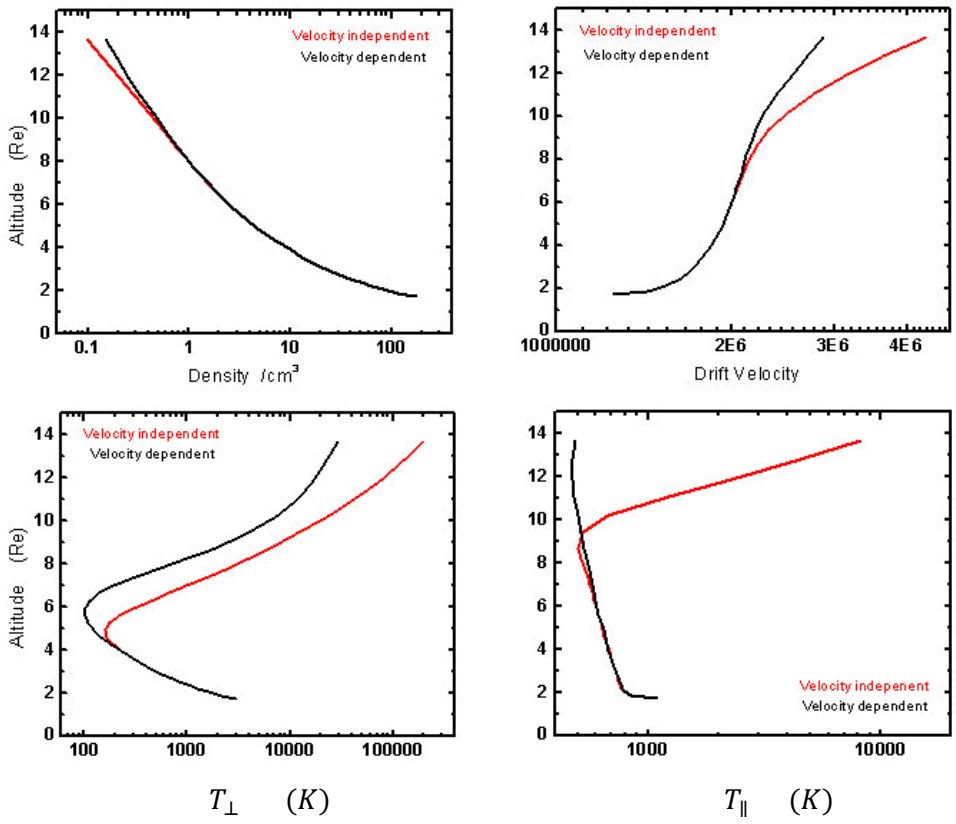

Figure 3.2 : The profile of H^+ moments as a function of altitude according to RCC model, including altitude and velocity dependent WPI in black and the altitude dependent in red color, the lower order moments are: density $n(H^+)$, drift velocity $u(H^+)$, perpendicular temperature $T_{\perp}(H^+)$,and parallel temperature $T_{\parallel}(H^+)$, at the top left, top right, bottom left and bottom right respectively.

3.3: Barghouthi model:

Barghouthi model as mentioned in chapter 2, explains the heating process for ions at high latitudes and altitudes by improving the velocity diffusion coefficient ($D_{\perp}$) model, [Barghouthi, 1997] introduce the altitude dependent diffusion coefficient, as a function of geocentric distance ($\frac{r}{R_E}$), where the final expression for $D_{\perp}$ is a function of velocity and altitude as in equation 2.20 . The output results based on Barghouthi model Presented in Fig (3.3) in the next page.

The results of velocity distribution function at different altitudes for H^+ is represented down in Fig (3.3), where the electromagnetic wave length which used in the simulation is 8 km, we can see that at the exobase the maxwellian feature because there is no clear effect for wave particle interaction at the low altitudes where the gyroradius is small comparison with electromagnetic waves length, at 3.9 R_E parallel velocity start to be greater than perpendicular where the gyroradius still smaller than electromagnetic waves, so in the absence of wave particle interaction body forces will dominant on the ions behavior, so the perpendicular adiabatic cooling will be effective, this behavior is dominant to 5.6 R_E, then wave particle interaction start balance from 5.9 R_E to 6.6 R_E , at 8.1 R_E the anisotropy be clear and the conic shape is obvious and dominant until 11.1 R_E where the perpendicular velocity greater than the parallel due to WPI which heat the ions in perpendicular direction and that make mirror force more effective, at 11.9 R_E the toroidal feature start to appear, and be more obvious at 12.8 R_E and 13.7 R_E to give saturation at higher altitudes due to absence of perpendicular heating, mean the distribution function shape invariable because the most of ions leave the significant heating altitudes [Barghouthi, 2007], so the heating process will exhibits self limitation [Barghouthi and Atout, 2006].

Figure 3.3 : H^+ ions velocity distribution function in the polar region according to Barghouthi model, we get results at 28 different altitude , we start from 1.7 Re geocentric distance to 13.7 Re, for 8 km electromagnetic wavelength ($\lambda_{\perp}$), the distribution function for H^+ ions represented by equal values contours in the normalized velocity plane ($c_{\parallel}$, $c_{\perp}$), where $c = \frac{[v-u(H^+)]}{[\frac{2kT(H^+)}{m(H^+)}]^{1/2}}$. (next page)

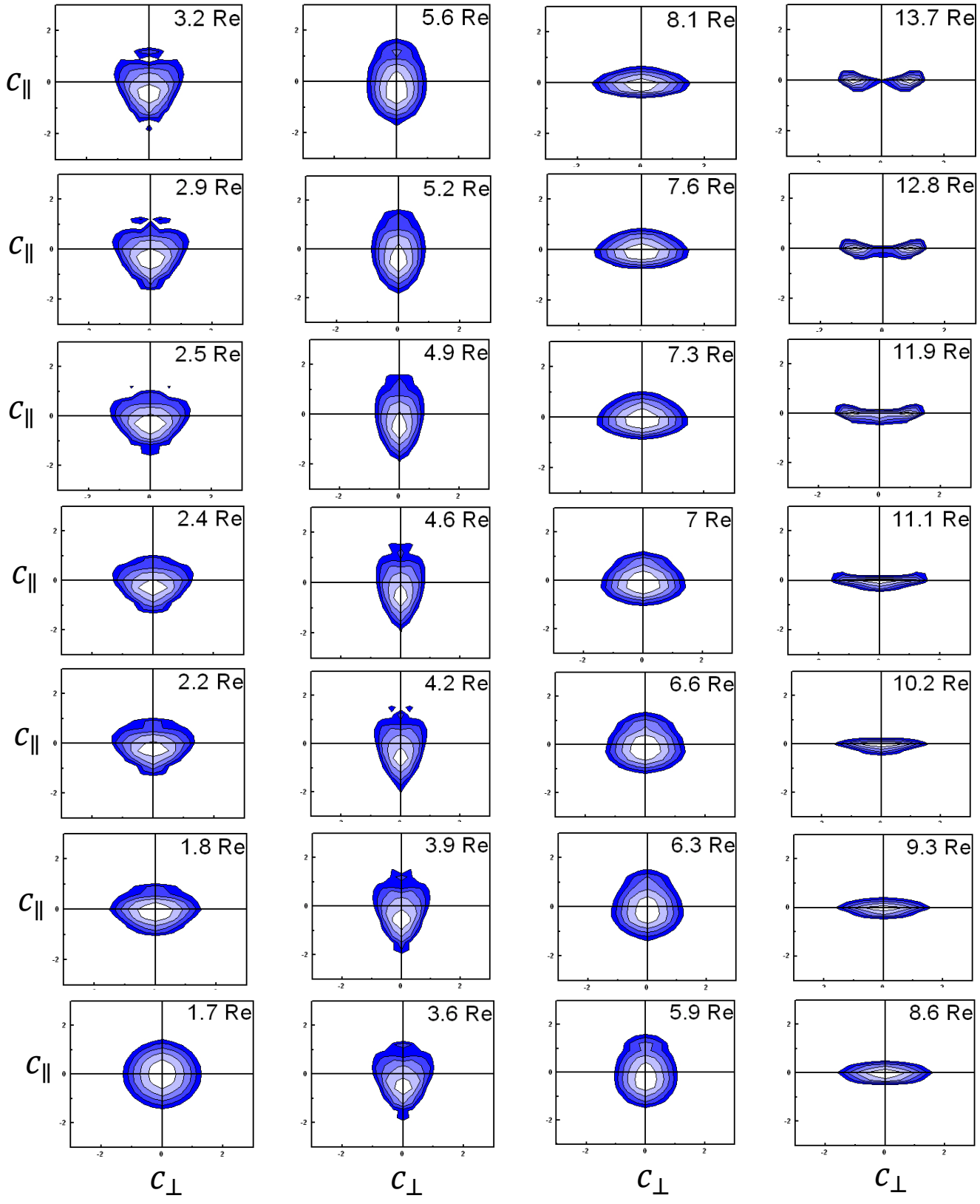
3.2 Re
5.6 Re
8.1 Re
13.7 Re
2.9 Re
5.2 Re
7.6 Re
12.8 Re
2.5 Re
4.9 Re
7.3 Re
11.9 Re
2.4 Re
4.6 Re
7 Re
11.1 Re
2.2 Re
4.2 Re
6.6 Re
10.2 Re
1.8 Re
3.9 Re
6.3 Re
9.3 Re
1.7 Re
3.6 Re
5.9 Re
8.6 Re
$c_{\parallel}$
$c_{\perp}$

To understand toroidal shape formation for velocity distribution function we will turn back to equation 2.20, we will get high values (the peak) for $D_\perp$ when $v_\perp$ approach to zero , the $D_\perp$ will rapidly decrease for large values of perpendicular velocity $v_\perp$ so the particles will diffuse out of the high $D_\perp$ region of phase space to accumulate in relatively low $D_\perp$ region, and forming the toroidal shape of velocity distribution function.

To study the profile of H^+ ion moments we represent the results of the density, drift velocity, parallel temperature and perpendicular temperature, as a functions of altitude as shown in Fig (3.4) , where the wavelength used in calculation is 8 km, the altitudes from 1.7 Re to 13.7 Re.

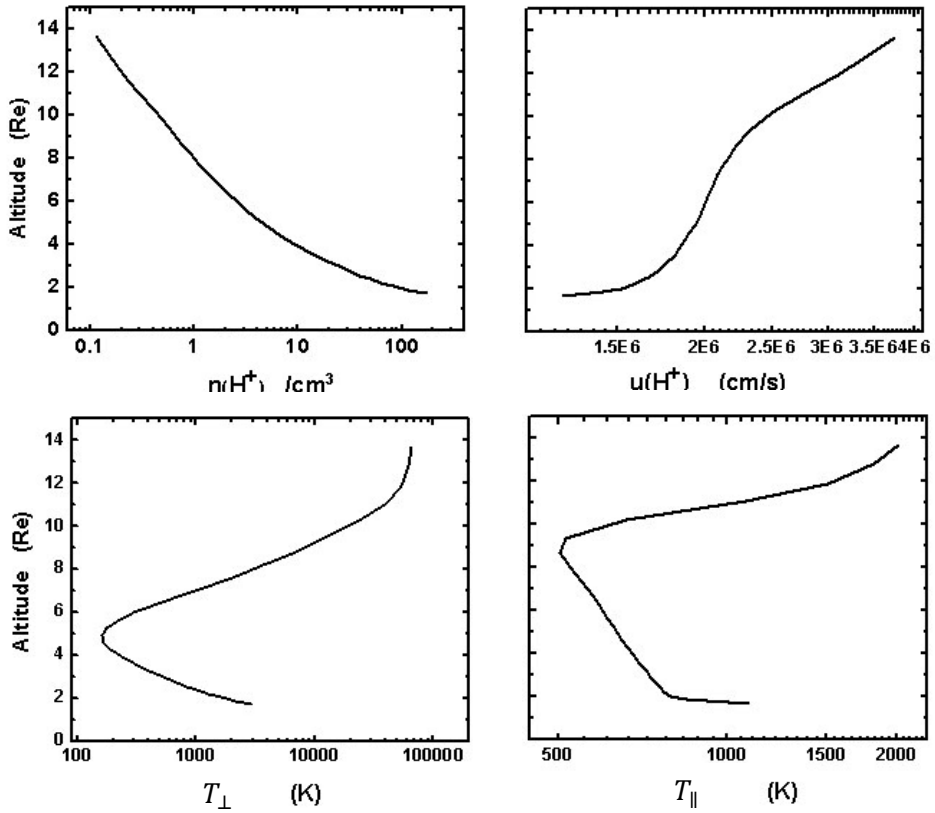

Figure 3.4 : The profile of H+ moments as a function of altitude according to Barghouthi model, the lower order moments are: density n(H^+), drift velocity u(H^+), perpendicular temperature $T_\perp$,and parallel temperature $T_\parallel$, at the top left, top right, bottom left and bottom right respectively.

The drift velocity for H^+ ions increases with altitude, because as altitude increases the effect of wave particle interaction will rise and the perpendicular heating will increase and the upward mirror force will be more affective, that will increase the drift velocity, then when the wave particle interaction is dominant the increases of velocity will be more rapid, to reach a saturation region when the most of ions moves from high $D_\perp$ to low $D_\perp$ region and the WPI will be negligible and the mirror force decreases, that leads to decrease the upward acceleration.

By the flux limiting flow ($\tilde{n}\,\tilde{u} = 1$) , the net escape flux is constant then it's acceptable that increasing of drift velocity will accompany with decreasing in ion density, as shown in Fig (3.3) top left and top right .

The perpendicular temperature (bottom left) exhibit a competitional behavior between the perpendicular heating due to WPI and the perpendicular adiabatic cooling, we can see from the figure that the $T_\perp(H^+)$ decreases with altitude up to 5 Re, since the adiabatic cooling is dominant at low altitudes, at higher altitudes the perpendicular heating due to WPI dominant and reverse the process by increaseing $T_\perp(H^+)$ rapidly, with increasing altitude the ion gyroradius will be in order of electromagnetic wavelength and $D_\perp$ will be small, so WPI will be negligible and the perpendicular temperature increases slowly to reach a saturation state.

In the bottom right panel we have the out put of parallel temperature profile, we see that at low altitudes the parallel temperature decreases with altitude by the parallel adiabatic cooling, but around 8 Re we see rapid increasing of $T_\parallel(H^+)$.

The $T_\parallel(H^+)$ governed by velocity dependant WPI by many sides, the first issue is the correlation between $T_\perp(H^+)$ and $T_\parallel(H^+)$, since increasing $T_\perp(H^+)$ will increase the parallel outflow velocity by the mirror force, the second one is the heat transfer from perpendicular to parallel direction due to the divergence of geomagnetic field and the parallel adiabatic cooling due to the increase in the drift velocity of H+ ions (Barakat and Lemaire, 1990).

If we cogitate the Fig (3.3) and Fig (3.4) we will note the harmony between them.

3.4. Bouhram model:

Bouhram model explained in section 2.7.3 which built on special understood for wave particle interaction by an altitude and velocity dependant expression for perpendicular velocity diffusion coefficient, this expression for polar region was inserted in equation 2.24 .

Figure 3.5 represents the output of simulation based on Bouhram expression, this figure consists of velocity distribution function for 28 different altitudes extended from 1.7 Re to 13.7 Re , the electromagnetic wavelength which used in simulation is 8 km, the velocity distribution function for the exobase at 1.7 Re is Maxwellian by the boundary conditions, then the anisotropy feature start to form at 3.9 Re then dominate up to 5.6 Re under the dominant of perpendicular adiabatic cooling, where the wave particle interaction valuable activity and dominant is not yet, where at low altitudes $\frac{k_{\perp 0} v_{\perp}}{\omega_c} << 1$ then $J_0 \sim 1$ by refer to equation 2.24 and that mean $D_{\perp}$ in this case is altitude dependent and velocity independent by unity of Bessel function term , while for higher altitudes the Larmor radius will be comparable with electromagnetic wave length, so at 7 Re the wave particle interaction emerge and reform the velocity distribution function in conic shape showing the perpendicular heating process print, this shape will ripen at 8.6 Re, the conic feature developed by the altitude dependent wave particle interaction, by perpendicular heating for H^+ ions this feature will dominate until 11.1 Re, in this region velocity independent wave particle interaction and upward mirror force control the process.

At 11.9 Re the toroidal feature start to form and well clear at 12.8 Re and 13.7 Re to saturate above at the higher altitudes, this feature can explain by Bouhram concept from equation 2.24, where the valuable $D_{\perp}$ (peak) happened when the perpendicular velocity approach to zero, and by increasing of perpendicular velocity to large values the $D_{\perp}$ will decreases rapidly by factor of $J_0^2\left(\frac{k_{\perp 0} v_{\perp}}{\omega_c}\right)$, since the ions tend to move from high $D_{\perp}$ to accumulate in low $D_{\perp}$ forming the toroidal shape.

So at high altitudes the value of $D_{\perp}$ will be small and the wave particle interaction will be negligible, because the value of $\frac{k_{\perp 0} v_{\perp}}{\omega_c} > 1$ because the gyro radius $\frac{v_{\perp}}{\omega_c}$ increases with altitude by decreasing of geomagnetic field with altitude, then $D_{\perp}$ decreases by decreasing of Bessel

function factor, since the important role is to body forces like gravity, mirror force and polarization electric field, that described by Liouville theorem [Barakat and Scunk, 1982].

Figure 3.5 : H+ ions velocity distribution function in the polar region according to Bouhram model, the results at 28 different altitude , we start from 1.7 Re geocentric distance to 13.7 Re, for 8 km electromagnetic wavelength ($\lambda_{\perp}$), the distribution function for H+ ions represented by equal values contours in the normalized velocity plane ($c_{\parallel}$, $c_{\perp}$), where $c = \frac{[v-u(H^+)]}{[\frac{2kT(H^+)}{m(H^+)}]^{1/2}}$ (next page).

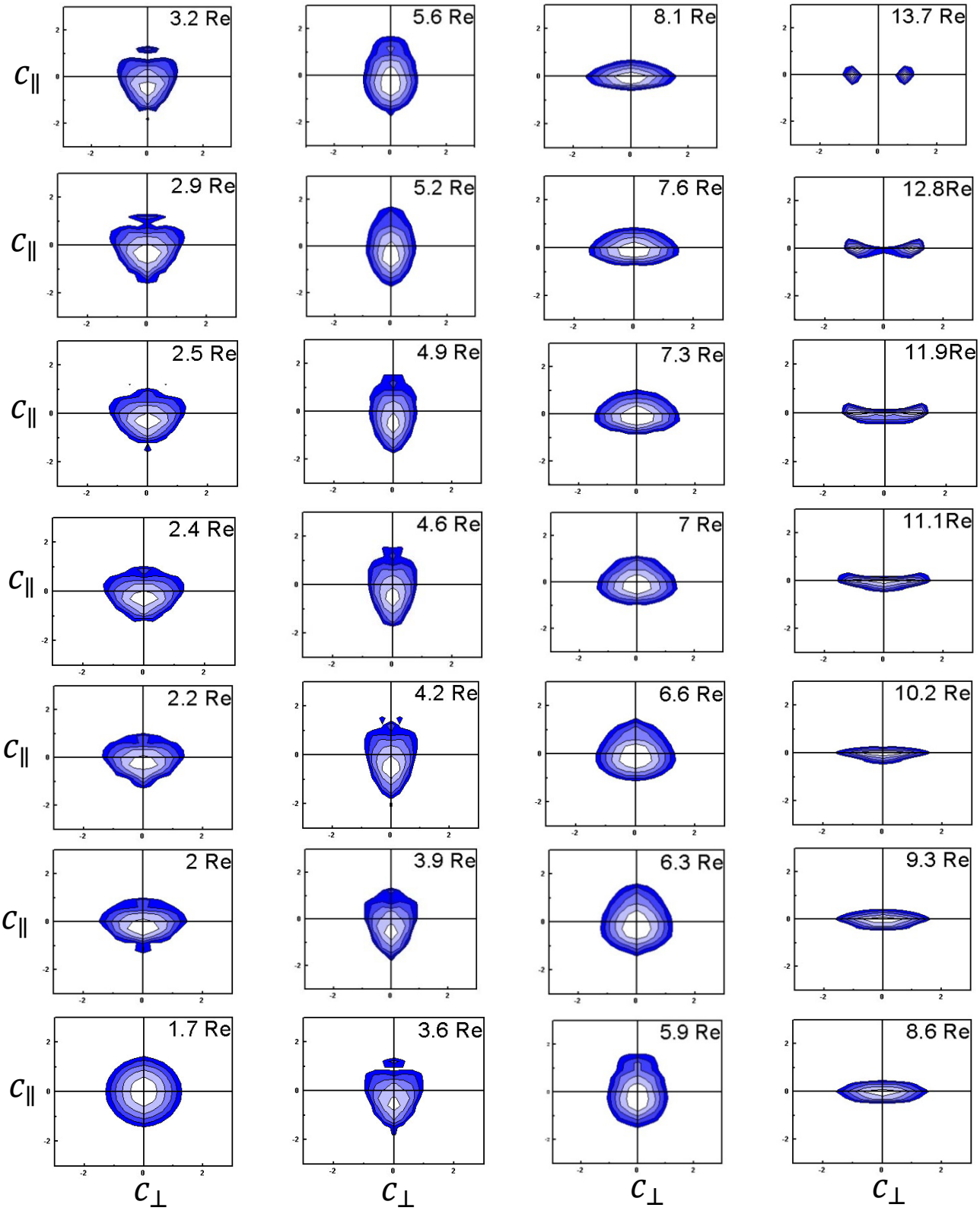
3.2 Re
5.6 Re
8.1 Re
13.7 Re
2.9 Re
5.2 Re
7.6 Re
12.8Re
2.5 Re
4.9 Re
7.3 Re
11.9Re
2.4 Re
4.6 Re
7 Re
11.1Re
2.2 Re
4.2 Re
6.6 Re
10.2 Re
2 Re
3.9 Re
6.3 Re
9.3 Re
1.7 Re
3.6 Re
5.9 Re
8.6 Re
$c_{\parallel}$
$c_{\perp}$

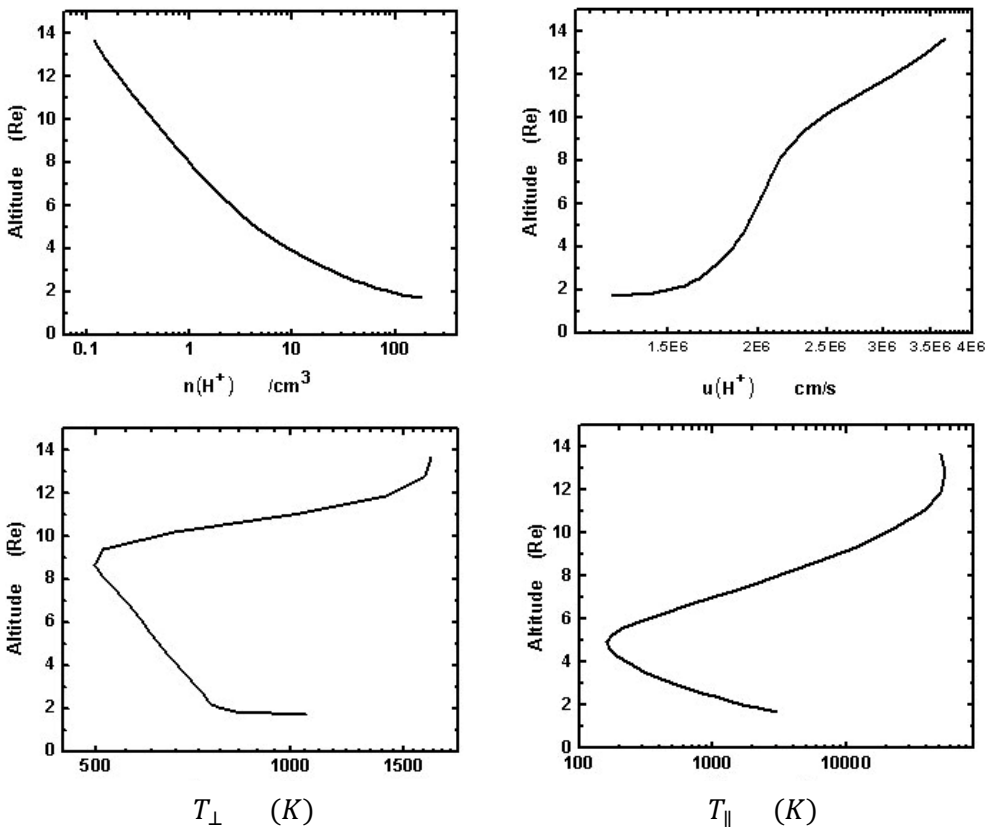

Figure 3.6 : Altitude profile of H^+ lower order moments according to Bouhram model for 8 km electromagnetic wavelength, the lower order moments are: density $n(H^+)$, drift velocity $u(H^+)$, perpendicular temperature $T_\perp$,and parallel temperature $T_\parallel$, at the top left, top right, bottom right and bottom left respectively.

Figure 3.6 above gives us the results of main moments for H^+ under the effect of wave particle interaction, the density altitude profile (left top) show normal decreasing with altitude by the gravity, but we can note that at highest altitudes the decreasing rate will slow, this slowing due to decreasing of drift velocity acceleration because density and drift velocity inversely related to keep the constant escape flux, the drift velocity profile is shown in figure 3.6 right top, at low altitudes we see low rate of velocity increasing with altitude, because at low altitudes the gyroradius $\frac{v_\perp}{\omega_c}$ is small with strong magnetic field, so the argument $\frac{k_{\perp 0} v_\perp}{\omega_c} << 1$ then $J_0 \sim 1$, that mean the wave particle interaction is velocity independent, but the

perpendicular heating will be more clear upper with increasing the velocity rapidly with altitude, for highest altitudes we can note from top right of figure 3.6 the slowing of velocity acceleration, this behavior because the gyroradius will increase to be relative to electromagnetic wavelength so the value of $\frac{k_{\perp 0} v_{\perp}}{\omega_c} > 1$, so the perpendicular velocity diffusion coefficient decreases and the heating process will be limited and the acceleration rate will decreases tending to saturation.

The altitude profile for perpendicular temperature is presented at the bottom right of figure 3.6 , at the lower altitudes up to 5 Re the perpendicular adiabatic cooling is dominant, then the wave particle interaction start to inverse the process to heating process in perpendicular plane by velocity independent wave particle interaction, at highest altitudes the increasing rate for perpendicular temperature $T_{\perp}$ will be limited at 11 Re to reach saturation (invariant of $T_{\perp}$ with altitude) at 12 Re and 13 Re, this behavior is an obvious argument for velocity dependent wave particle interaction effect, while at high altitudes $\frac{k_{\perp 0} v_{\perp}}{\omega_c} > 1$ as explained above, and the ion's motion under the body forces and mirror force.

Parallel temperature profile (bottom left) exhibit decreasing in temperature with altitude under effect of the parallel adiabatic cooling dominant, this behavior start rapidly then the rate decreases but still effect up to 9 Re then the dominant of wave particle interaction inverse this behavior by increasing of temperature with altitude, then to saturate at 12 Re due to effect of velocity dependent wave particle interaction, this behavior happened under indirect WPI effects [Barakat and Barghouthi, 1994], while the upward mirror force support the adiabatic cooling, that is clear at low altitudes where the mirror force effective by strong gradient of geomagnetic field lines, and the correlation between $T_{\perp}$ and $T_{\parallel}$ is clear if we investigate two bottom panels in Fig (3.6) , we can see the correlative and sometime simultaneously increasing of temperature , because the energy transfer from perpendicular to parallel direction.

Chapter Four

Comparison and Conclusion

Chapter Four : Comparison and Conclusion

The comparison in this chapter will be in two parts, the first part will compare between the simulation of the three Monte Carlo models, the difference between models refers to diffusion coefficient formula in each model, Fig (4.1) represents the velocity distributions at different altitudes, for the three models, RCC, Barghouthi, Bouhram, while Fig (4.2) represents the altitude profile of H^+ moments density, drift velocity, perpendicular and parallel temperatures. In the second part we will compare our results in polar wind with those in the Auroral region [Barghouthi, 2008], the comparison will be for each model separately, the moments profile as a result of RCC model, Barghouthi model and Bouhram model will display respectively in Fig (4.3), Fig (4.4), Fig (4.5).

4.1. Comparison between the three models in the polar wind:

Fig (4.1) presents the H^+ velocity distribution for the three models and for the velocity independent WPI, all models start at 1.7 Re with Maxwellian distribution, then the anisotropy appear $T_\perp(H^+) > T_\parallel(H^+)$ developing the conic shape with altitude due to perpendicular heating by wave particle interaction, the similarity between Barghouthi and Bouhram models with velocity independent WPI at low altitudes is clear, while RCC model exhibit a different behavior as $T_\parallel(H^+) > T_\perp(H^+)$ due to adiabatic cooling and exhibit weakness of wave particle interaction at this altitudes, at higher altitude (more than 9.3 Re) all models gives perpendicular heating dominant reach to saturation , the toroidal shape shown in all models at very high altitudes, but the toroidal shape in Bouhram is more extreme than Barghouthi model , while the velocity independent don't produce a toroidal shape and saturate at conic shape.

Figure 4.1 : Velocity distribution function of H^+ ions in the polar region, consist of four results, velocity independent wave particle interaction and three velocity dependent models, RCC, Barghouthi and Bouhram, for 7 different altitudes, the distribution function for H^+ ions represented by equal values contours in the normalized velocity plane ($\tilde{c}_\parallel$, $\tilde{c}_\perp$), (next page)

Velocity independent WPI	RCC	Barghouthi	Bouhram

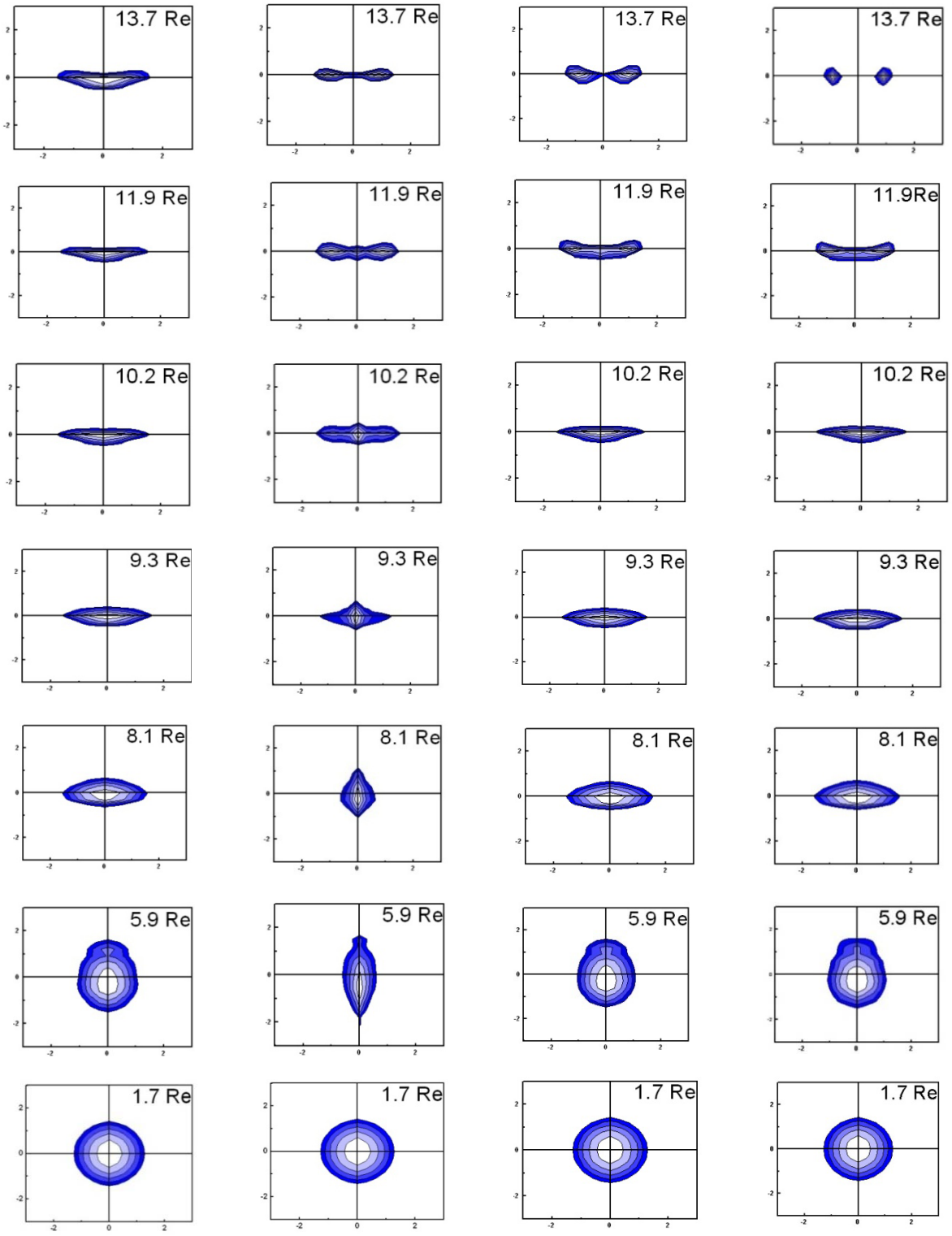

The low order velocity moments for all models and velocity independent WPI are represented in Fig (4.2) for comparison, the drift velocity profile (top right) show that all curves are similar up to 7 Re where the divergence of the curves be clear at higher altitudes due to different in $D_{\perp}$ equations, so different velocity dependence wave particle interactions and different high altitude behavior, from the figure we note a low increasing of drift velocity at high altitudes in RCC curve (dashed red) due to rapid decreasing in $D_{\perp}$ at high altitudes as factor of $\left(\frac{v_{\perp}}{v_0}\right)^{-3}$ in eq (2.22), where Barghouthi and Bouhram models exhibit more increasing in velocity at high altitudes, the velocity independent curve (solid black) gives high increasing of drift velocity.

The behavior of drift velocity curves determine the behavior of density profile, so the RCC gives higher densities at high altitudes to compensate the low increasing rate of velocity, because the net escape flux is constant, in contrast with velocity independent curve, while Bargouthi (dotted green) and Bouhram (dashed dotted blue) exhibit similarity in moderation as in drift velocity profile.

For the perpendicular temperature (bottom left) the similarity of all curves up to 4 Re, then the WPI be dominant and inverse the process by increasing the perpendicular heating with altitude , RCC curve show clear different with weak perpendicular heating, while Barghouthi and Bouhram curves are closed to each other and shows saturation in perpendicular heating at high altitudes above 10 Re with more soft saturation in Barghouthi curve, but the velocity independent can't produce any velocity dependant changes at high altitudes and continue in increasing at the same rate.

For the parallel temperature profile in the bottom right one, where the competition between parallel adiabatic cooling and energy transfer from perpendicular direction to parallel one, we see common behavior in parallel adiabatic cooling dominant at low altitudes, then the wave particle interaction correct this behavior up to 9 Re in common behavior also, the different path for the graph start above 9 Re, where the velocity dependent $D_{\perp}$ for each model affect the behavior, so the effect of velocity dependent WPI will decrease the transfer of energy from perpendicular to parallel direction, in RCC case we see a poor energy transform from perpendicular to parallel direction, and has a weak perpendicular temperature as shown in bottom left, where the velocity independent show continuous increasing of parallel

temperature, while Barghouthi (dotted green) and Bouhram (dashed dotted blue) exhibit velocity dependent WPI decreases the energy transfer from perpendicular to parallel direction.

Figure 4.2 : The profile of H^+ moments as a function of altitude consisting of velocity independent WPI (solid black), and three velocity dependent models , RCC (dashed red), Barghouthi (dotted green), Bouhram (dashed dotted blue). The lower order moments are: density $n(H^+)$, drift velocity $u(H^+)$, perpendicular temperature $T_\perp$,and parallel temperature $T_\parallel$, at the top left, top right, bottom left and bottom right respectively.

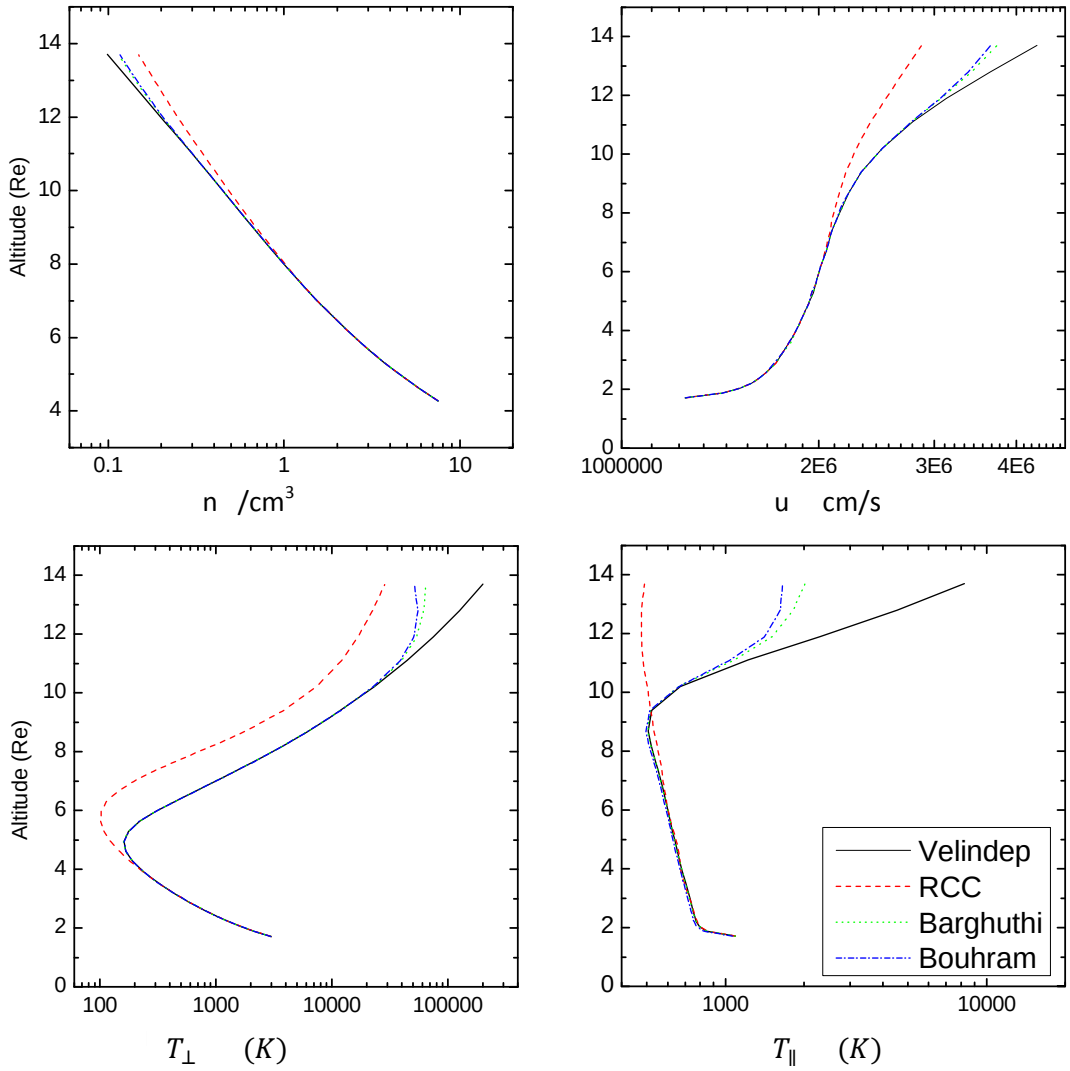

4.2. Comparison between Polar and Auroral ion outflow:

The results of our simulation in polar wind are compared with ion outflow in the auroral region which is more active, so the comparison between polar wind and it's surrounded aurora will give more comprehensive for ionosphere magnetosphere coupling at high latitudes and high altitudes, the low order velocity moments in polar wind which discussed in previous section and auroral low order velocity moments [Barghouthi 2008], will present for our three models for comparison.

Fig (4.3) represent the low order velocity moments for RCC model in polar (black) and auroral region (red), the drift velocity behavior in the top right show higher values in aurora region, there is a low acceleration for particles at low altitudes in aurora compared to the same altitudes in the polar wind, but for higher altitudes above 2 Re the velocity quickly increases in aurora, where it's slowly increases in polar wind region, this velocity different for the benefit of aurora according to high observation levels of electromagnetic turbulences in aurora than polar wind region [Chang et al., 1986], that's mean higher wave particle interaction in aurora.

This high drift velocity in aurora will inverse in density profile to keep a constant net escape flux [Barghouthi, 1997], the decreasing of density with altitude exhibit similar behavior in each regions with higher values in polar cap region.

For perpendicular temperature comparison (left bottom) we see perpendicular adiabatic cooling dominant for 6 Re in the polar wind, while this dominant disappear at 2 Re in the aurora, and the increasing of perpendicular temperature dominate from lower altitudes than polar wind, the temperatures in aurora is higher than polar wind, that mean the wave particle interaction is stronger in aurora and dominant at lower altitudes.

The right bottom one show the parallel temperature comparison profile, there is no harmony between aurora and polar wind, in the polar wind the parallel adiabatic cooling is strong competitor for energy transform from perpendicular to parallel direction, so the parallel adiabatic cooling superior in all altitudes in polar wind, while that inverse from 4 Re at the aurora and the energy transform from perpendicular to parallel direction is dominant.

Figure 4.3 : Altitude profile of H^+ moments according to RCC model for polar wind (black) and Aurora (red), the lower order moments are: density $n(H^+)$, drift velocity $u(H^+)$, perpendicular temperature $T_\perp$,and parallel temperature $T_\parallel$, at the top left, top right, bottom left and bottom right respectively.

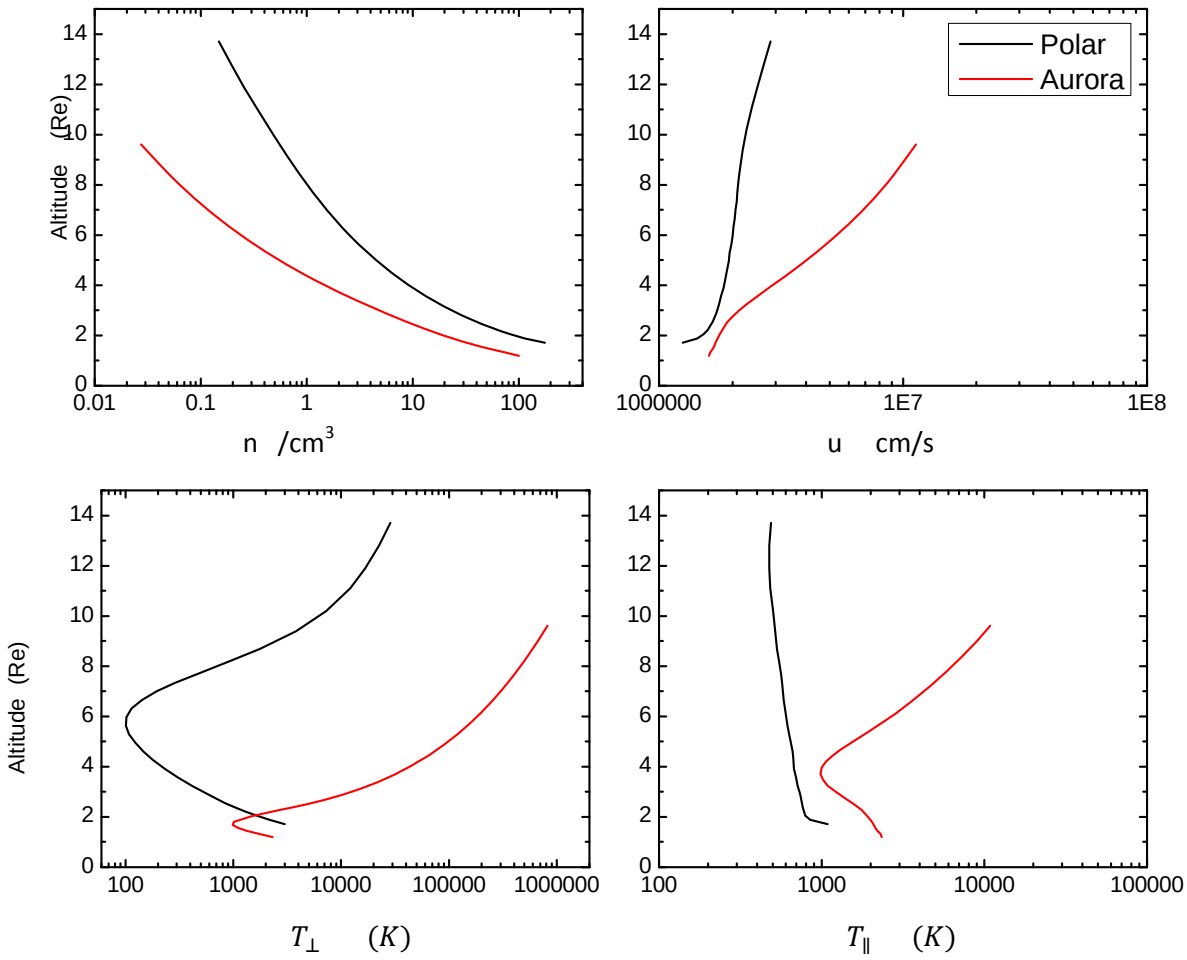

For Barghouthi model we insert the results of low order velocity moments in Polar cap region and Auroral region in Fig (4.4) to compare between this two ion outflow regions, at the top right, the drift velocity profile with altitude, for Polar region we see low increasing rate of drift velocity which mean low energize for charged ions comparison with the Auroral region which exhibit high acceleration for charged ions above 2 Re, and saturate above 6 Re due to velocity dependent WPI, this saturation velocity in Auroral region missed in RCC figure.

The density profile is a mirror of drift velocity, because the constant net flux escape for ion outflow. And the effect of body force which decrease the escape ions due to gravity, so the density of charged particles decreases with altitude, the density at the Polar cap is higher than Auroral region.

The behavior of perpendicular temperature at Polar region is completely different from Auroral region, in the Polar cap region the perpendicular adiabatic cooling dominate up to 5 Re, while at Aurora the adiabatic cooling effect rapidly disappear before 2 Re and the perpendicular temperature increasing due to strong perpendicular heating, and strong wave particle interaction, the saturation around 4 Re due to velocity dependent WPI.

The parallel temperature profile exhibit an abrupt adiabatic cooling dominant in Polar and Auroral regions, above 2 Re wave particle interaction start to effect timidly in Polar cap region, while it's effect in Aurora strongly rise the parallel temperature by heat transfer from perpendicular to parallel by mirror force, there is clear harmony between perpendicular and parallel temperature in polar and Auroral regions.

Buhram comparison in Fig (4.5) gives a data approach to Barghouthi results with some detail differences, the velocity drift in Bouhram at Aurora increasing with higher rate than in Barghouthi model, and the parallel temperature saturate at in Barghouthi model lower temperatures than in Bouhram, this difference is clear in Auroral region more than in Polar cap region.

Figure 4.4 : Altitude profile of H^+ moments according to Barghouthi model for polar wind (black) and Aurora (red), the lower order moments are: density $n(H^+)$, drift velocity $u(H^+)$, perpendicular temperature $T_\perp$,and parallel temperature $T_\parallel$, at the top left, top right, bottom left and bottom right respectively.

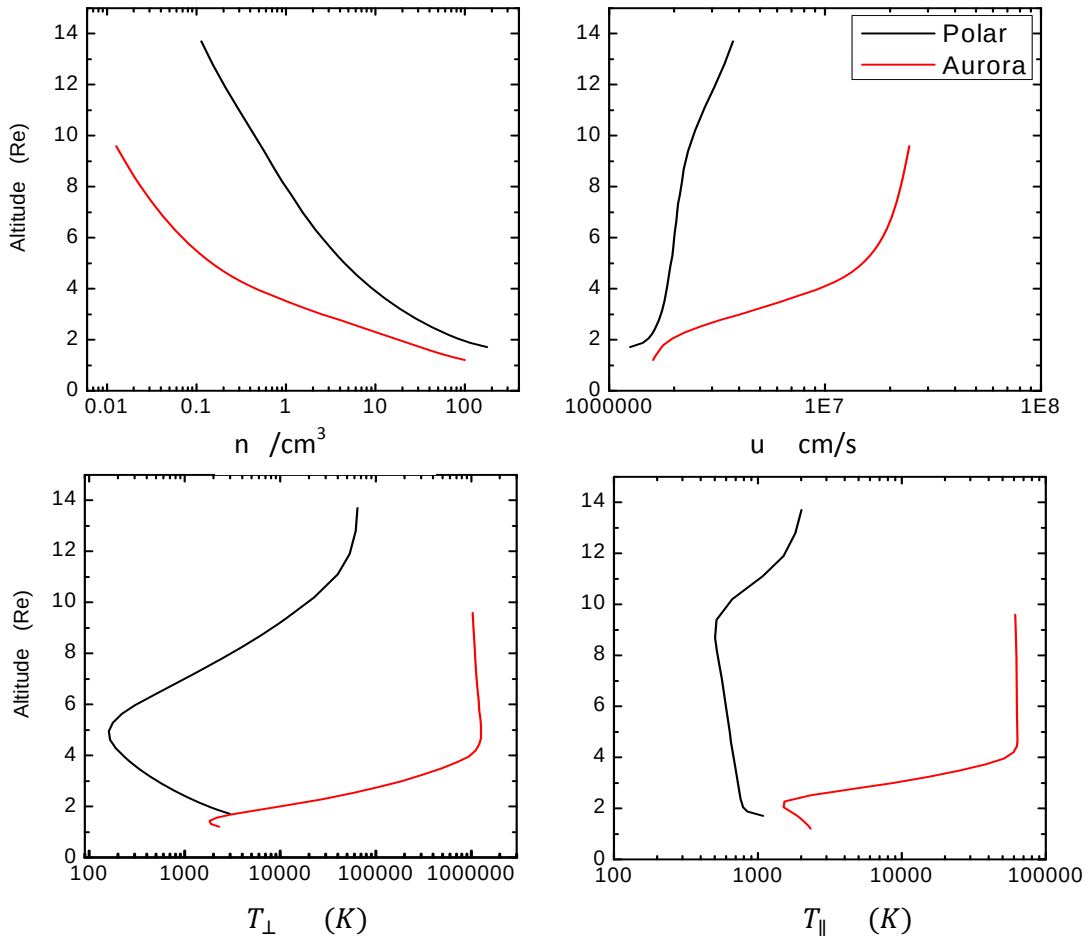

Figure 4.5 : Altitude profile of H^+ moments according to Bouhram model for polar wind (black) and Aurora (red), the lower order moments are: density $n(H^+)$, drift velocity $u(H^+)$, perpendicular temperature $T_\perp$,and parallel temperature $T_\parallel$, at the top left, top right, bottom left and bottom right respectively.

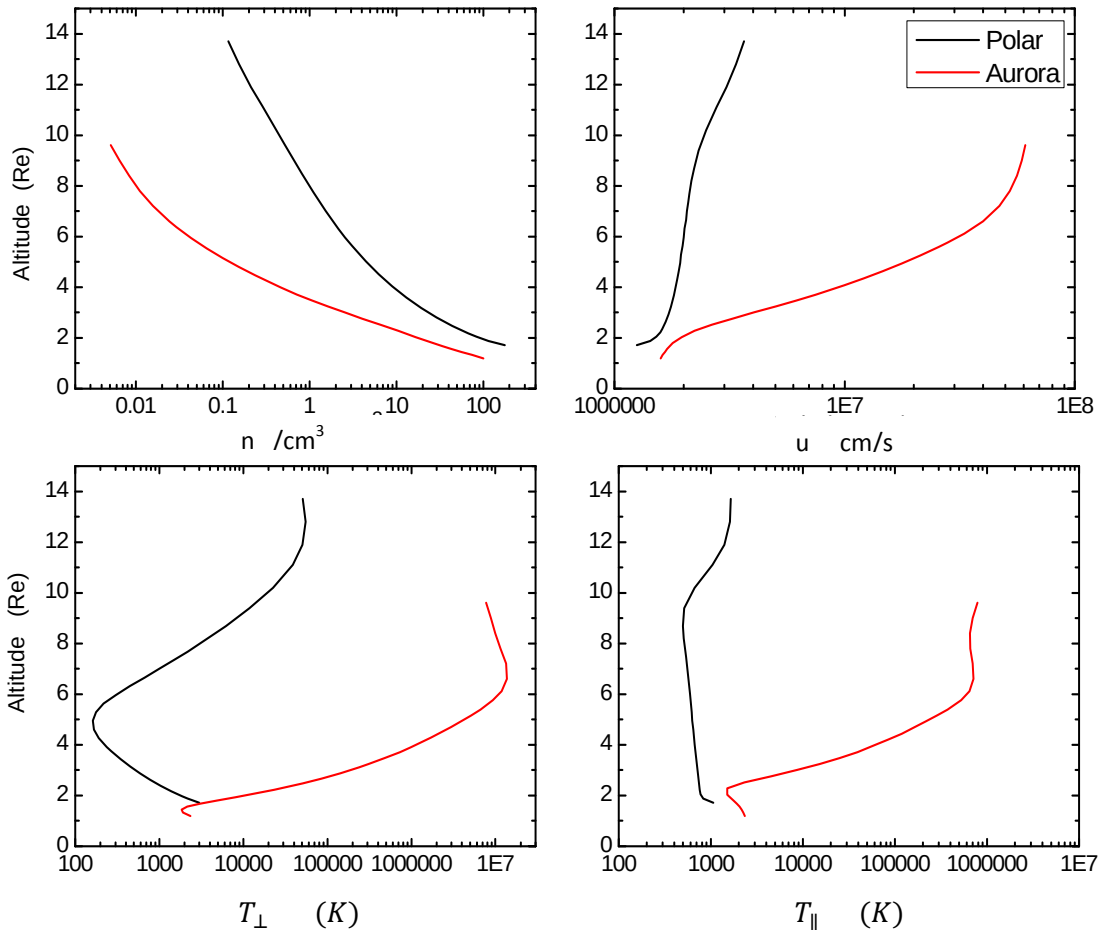

4.3. Conclusion :

Velocity distribution function for hydrogen ions (H^+) were produced, and the low order velocity moments, drift velocity, density, perpendicular temperature and parallel temperature for Bouhram model for 28 different altitudes and reproduce that for Barghouthi and RCC models to compare the produced results with other to reach for better understanding of space plasma physics at the regions of ions outflow, and to choose the most suitable one , or forming a new one make a summary of them and use the powerful part in each one.

The most important part of our simulation (Monte Carlo) is the different of definition of (altitude and velocity wave particle interaction) between these models, the simulation done in Polar cap region for hydrogen ions (H^+), while the other effects are included in calculation, like polarization electric field, diverging geomagnetic field and the gravity.

The following could be concluded:

1 - The velocity dependent wave particle interaction reduce the ions velocities at high altitude , and saturate the temperature at high altitudes.

2 - At low altitudes the velocities is low, and the argument is much less than unity, $\left(\frac{k_{\perp 0} v_{\perp}}{\omega_c}\right) \ll 1$, so the results are independent of the electromagnetic turbulence wave length.

3 - At intermediate altitudes the wave particle interaction become dominant and the perpendicular heating process produce the conic shape.

4 - Above the saturation altitude this argument $\left(\frac{k_{\perp 0} v_{\perp}}{\omega_c}\right)$ be greater than unity and the perpendicular heating turned to be negligible, producing toroidal feature .

5 - RCC gives a different behavior compared to other models, always produce saturation earlier than the other models, and small increasing rate for drift velocity and low perpendicular temperatures and no parallel temperature increasing rate, which reflect low wave particle interaction formula.

6 - Barghouthi and Bouhram exhibit similar behavior for hydrogen ions in Polar cap region.

7 - The velocity of polar wind hydrogen ions increases with altitudes and have large velocities at high altitude.

8 - The Aurora has a strong wave particle interaction comparison with Polar cap region, due to strong electromagnetic wave turbulences.

9 - The temperature and velocities of Auroral hydrogen ions are greater than polar wind.

10 - As a result of the comparison between the models, it's difficult to choose the appropriate model, an observations at very high altitudes is needed to give an evidence to choose the most appropriate.

4.4. Further work:

1. Make an explanation study for the different models, based on different approximations and assumptions between models. This study could aim to give the physical and mathematical explanation for the differences.

2. An explanation study could be established to help in forming a new model make a summary of them and use the powerful part in each model.

3. Obtain an observation for H^+ velocity distribution function at very high altitudes, more than 8Re to compare between models and observation to determine the most appropriate.

4. Produce data for O^+ ions in the polar cap region for Bouhram model and make a comparison between models, and comparison with observation if available.

References :

Abe, T., B. A. Whalen, A. W. Yau, R. E. Horita, S. Watanbe, and E. Sagawa, **EXOS D (Akebono) Superathermal mass spectrometer observations of the polar wind**, J. Geophys. Res., 98, 11, 191, 1993a.

Abe, T., et al., **Observations of polar wind and thermal ion outflow by Akebono/SMS**, J. Geomagn. Geoelectr., 48, 319-325, 1996.

Abe, T., et al., **Long-term variation of the polar winds velocity and its implication for the ion acceleration process: Akebono/suprathermal ion mass spectrometer observations**, J. Geophys. Res., 109, A09035, 2004.

Aldrich C., **Particle code simulations with injected particles**, Space science reviews, 42, 131, 1985

Axford, W. I., and C. O. Hines, **A unifying theory of high-latitude geophysical phenomena and geomagnetic storms**, Can. J. phys., 39,433,1961.

Axford, W. I., **The polar wind and the terrestrial helium budget**, J. geophys. Res., 73, 6855, 1968.

Banks, P. M., and T. E. Holzer, **The polar wind**, J. Geophys. Res., 73,6846-6868, 1968.

Banks, P. M., and T. E. Holzer, **High- latitude plasma transport: The polar wind**, J. Geophys. Res., 74, 6317-6332, 1969b.

Barakat A. and R. Schunk, **Comparison of Maxwellian and bi-Maxwellian expansions with Monte Carlo simulations for anisotropic plasmas**, J. Phys. D, 15, 2189, 1982.

Barakat, A. R., and R. W. Schunk, **Effect of hot electrons on the polar wind**, J. Geophys. Res., 89, 9771-9783,1984.

Barakat A., and J. Lemaire, **Monte Carlo study of the escape of a minor species**, Phys. Rev. A, 42, 3291, 1990.

Barakat, A. R. and I. A. Barghouthi, **The effects of wave-particle interactions on the polar wind: Preliminary results**, Planet. Space Sci., 42, 987-992, 1994b.

Barbier, D., and D. Williams, **observations of the Aurora Borealis**, J. Geophys. Res., 55(4), 401-414, 1950.

Barghouthi, I. A., and A. R. Barakat, **Comparison between the wave-particle interaction in the polar wind and in the auroral region**, Phys. Space Plasmas, 13, 445– 450.1993.

Barghouthi I. A., **Effects of wave particle interactions on H^+ and O^+ outflow at high latitude; A comparative study**, J. Geophys. Res., 102, 22. 062-22.075, 1997.

Barghouthi I. A., A. R. Barakat, A. M. Persoon, **The effects of altitude –dependent wave particle interactions on the polar wind plasma,** Astrophysics and space sciences, 259, 117, 1998.

Barghouthi I. A., N. A. Qatanani, M.S. Abu Issa, **Toroidal distributions in the polar wind plasma**; Indian j.phys, 77B (6), 621-625, 2003a.

Barghouthi I. A., N. A. Qatanani, F. M. Allan, **Monte Carlo simulation of Boltzmann equation in space plasma at high latitudes**, Monte Carlo Methods and Appl., 9, 3, 201-216, 2003b.

Barghouthi, I. A., and M. A. Atout, **Monte Carlo modeling of toroidal ion distributions and ion temperatures at high altitudes equatorward of the cusp: Effect of finite gyroradius**, J. Geophys. Res., 111, A03202, 2006.

Barghouthi, I. A., N. M. Doudin, A. A. Saleh, and V. Pierrard, **High-altitude and high-latitude O^+ and H^+ outflows: the effect of finite electromagnetic turbulence wavelength** , Ann. Geophys., 25, 2195-2202, 2007.

Barghouthi, I. A., **A Monte Carlo study for ion outflows at high altitude and high latitude: Barghouthi model**, J. Geophys. Res., 113, A08209, 2008.

Belelly, P. L., A. R. Barakat, J. Fontari, D. Alcayde, M. Blancej. Wu, and C. Lathuillere, **Observations of the structure and vertical transport of the polar of upper ionosphere with the EISCAT VHF radar, 1, Is EISCAT able to determine O^+ and H^+ polar wind characteristics? A simulation study**, Ann. Geophys., 10,367-374, 1992.

Bouhram, M., M. Malingre, J. R. Jasperse, and N. Dubouloz , **Modeling transverse heating and outflow of ionospheric ions from the dayside cusp/clef: 1 A parametric study**, Ann. Geophys., 21, 1753–1771, 2003a.

Bouhram, M., M. Malingre, J. R. Jasperse, N. Dubouloz, and J.-A. Sauvaud, **Modeling transverse heating and outflow of ionospheric ions from the dayside cusp/clef: 2. Applications**, Ann. Geophys., 21, 1773–1791, 2003b.

Bouhram, M., B. Klecker,W. Miyake, H. Reme, J.-A. Sauvaud, M. Malingre, L. Kistler, and A. Blagau, **On the altitude dependence of transversely heated O^+ distributions in the cusp/cleft**, Ann. Geophys., 22, 1 –12, 2004.

Chandler, M.O., et al., Observations of polar ion outflows, J. Geophys. Res., 96, 1421-1428, 1991.

Chang, T., Coppi, B.: **Lower hybrid acceleration and ion evolution in the suprauroral region**, Geophys. Res. Lett., 8, 1253-1256, 1981.

Chang, T., Crew, G. B., Hershkowitz, N., Jasperse, J. R., Retterer,J. M., and Winningham, J. D.: **Transverse acceleration of oxygen ions by electromagnetic ion cyclotron resonance with broad band left-hand polarized waves**, Geophys. Res. Lett., 13, 636–639, doi:10.1029/GL013i007p00636, 1986.

Chapell, C. R., T. E. Moore, and J. H. Waite Jr., **The ionosphere as a fully adequate source of plasma for the earth's magnetosphere**, J. Geophys. Res., 92, 5896-5910, 1987.

Chen, M. W., and M. Ashour-Abdalla, **Heating of the polar wind due to ion-beam instabilities**, J. Geophys. Res., 95, 18, 949-18. 968, 1990.

Crew, G.B., T. Chang.: **Asymptotic theory of ion conic distributions**. Physics of fluids 28(8), 2382-2394, 1985.

Crew, G. B., T. Chang, J. M. Retterer, W. K. Peterson, D. A. Gurnett, and R. L. Huff, **Ion cyclotron resonance heated conics: Theory and observations**, J. Geophys. Res., 95, 3959 – 3985, doi:10.1029/JA095iA04p03959, 1990.

Demars, H.G., Schunk, R.W., **Semikinetic and generalized transport models of the polar and solar winds**, J. Geophys. Res., 97, 1581–1595, 1992.

Dessler, A. J., and F. C. Michel, **Plasma in Geomagnetic Tail**. J. Geophys. Res., 71, 1421, 1966.

Drakou, E., et al., **Ion temperature measurements from the Akebono suprathermal mass spectrometer: Application to the polar wind**, J. Geophys. Res., 102, 17523-17539, 1997.

E. Engwall, A. I. Eriksson, C. M. Cully, M. André, R. Torbert, and H. Vaith, **Earth's ionospheric outflow dominated by hidden cold plasma**, *Nature Geoscience*, *2*(1), 24–27, 2009.

Ganguli, S.B., **The polar wind**, Rev. Geophys., 34, 311-348, 1996.

Gosling, J., V. Pizzo, and S. Bame, **Anomalously Low Proton Temperatures in the Solar Wind following Interplanetary Shock Waves—Evidence for Magnetic Bottles**, J. Geophys. Res., 78(13), 2001-2009, 1973.

Gurnett, D. A., and U. S. Inan, **Plasma wave observations with the Dynamic explorer 1 spacecraft**, Rev. Geophys., 26, 285-316, 1988.

Huddleston, M. M., C. J. Pollock, M.P.Wuest, J. S. Pichett, T. E. Moore, and W. K. Peterson, **Toroidal ion distributions observed at high altitudes equatorwardof the cusp**, Geophysical, Research Letters, 27, 4, 469-472, 2000.

Lemaire, J., O^+, **H^+ and He^+ ion distributions in a new polar wind model**, J. Atoms. Terr. Phys., 34, 1647-1658, 1972.

Lemaire, J., and M. Scherer, **Kinetic models of the solar and polar winds**, Rev. Geophys., 11, 427-468, 1973.

Li, P., G. R. Wilson, J. L. Horwitz, and T. E. Moore, **Effect of mid-altitude ion heating on the ion outflow at polar latitudes**, Geophys. Res., 93, 9753-9763, 1988.

Moore, T. E., and D. C. Delcourt, **Transport and energization of ionospheric plasma** , Full Meet. Suppl., Eos Trans. AGU, 73(43), 471, 1992.

Nagai, T., J.H. Waite, J. L. Green, C. R. Chappel, **First measurement of supersonic polar wind in the polar magnetosphere**. Geophysical Research Letters 11, 669-672, 1984.

Nilsson. H., M. Waara, O. Marghitu, M. Yamauchi, R. Lundin, H. Rème, J.-A. Sauvaud, I. Dandouras, E. Lucek, L. M. Kistler, B. Klecker, C. W. Carlson, M. B. Bavassano-Cattaneo, and A. Korth**, An assessment of the role of the centrifugal acceleration mechanism in high altitude polar cap oxygen ion outflow,** Ann. Geophys., 26, 145-157, 2008.

Persoon, A. M., D. A. Gurnett, and S. D Shawhan, **polar cap electron densities from DE-1 plasma wave observations**, J. Geophys. Res., 88, 10, 123, 1983.

Pierrard, V., Lemaire, J., **A collisional kinetic model of the polar wind**, J. Geophys. Res., 103, 11701-11709, 1998.

Pierrard, V., Barghouthi I. A., **Effects of Wave-Particle Interactions on Double-Hump, Distributions of the H^+ Polar Wind**, Astrophysics and Space Science, 2005.

Retterer, J. M., Chang T., Crew, G. B., Jasperse J. R., and Winningham J. D., **Monte Carlo modeling of oxygen ion conic acceleration by cyclotron resonance**, phys. Rev. Lett., 59, 148-151, 1987a.

Retterer, J. M., Chang, T., Crew, Jasperse J. R., and J. D. Winningham, **Monte Carlo modeling of oxygen ion conic acceleration by cyclotron resonance with broadband electromagmetic turbulence,** in physics of space plasma, SPI Conf. Proc., pp.97-111, Scientific, Cambridge, Mass., 1987b.

Retterer, J., T. Chang, and J. Jasperse, **Transversely Accelerated Ions in the Topside Ionosphere**, J. Geophys. Res., 99(A7), 13189-13201, 1994.

Schunk R., **Mathematical structure of transport equations for multispecies flows**, Rev. Geophys., 15, 429, 1977.

Schunk, R.W. and D. S. Watkins, **Proton temperature anisotropy in the polar wind**, J. Geophys. Res.,87, 171-180, 1981.

Schunk, R. W., **The polar wind, in modeling Magnetospheric plasma**, Geophys. Monogr. Ser., Vol. 44, edited by T. E. Moore and J. H. Waite, P. 219, AGU, Washington, D. C., 1988.

Schunk, R.W., Sojka, J.J., **A three-dimensional time-dependent model of the polar wind**, J. Geophys. Res., 94, 8973-8991, 1989.

Schunk, R., and J. Sojka, **Global ionosphere□polar wind system during changing magnetic activity**, J. Geophys. Res., 102(A6), 11625-11651, 1997.

Schunk, R. W. and A. F. Nagy, Ionospheres: **physics plasma physics, and chemistry**, Cambridge, 2000.

Schunk, R.W., **Time-dependent simulations of the global polar wind**, J. Atmos. Solar Terr. Phys., this issue, 2007.

Skiff F, C S Ng, **A Bhattacharjee, W A Noonan and A Case, Wave-particle interaction,** Plasma Phys, 2000.

Su, Y.J., et al., **Polar wind survey with the Thermal Ion Dynamics Experiment/Plasma Source Instrument suite aboard POLAR**, J. Geophys. Res., 103, 29305-29337, 1988a.

Y.J. Su, J. Horwitz, T. Moore, B. Giles, M. Chandler, P. Craven, M. Hirahara, and C. Pollock, **Polar wind survey with the Thermal Ion Dynamics Experiment/Plasma Source Instrument suite aboard POLAR,** J. Geophys. Res., 103, A12, 1998.

Tam, S. W. Y., F. Yasseen, T. Chang, and S. B. Ganguli, **Self-consistent kinetic photoelectron effects on the polar wind**, Geophys. Res. Lett., 22(16), 2107-2110, 1995.

Tam S.W.Y., T. Chang, V. Pierrard, Kinetic modeling of the polar wind, 2007.

Tsurutani, B. T. and G. S. Lakhina, **Some concepts of wave- particle interactions in the collisionless plasmas**, Reviews of Geophysics, 35, 4, 491-502, 1997.

Wilsson, G. R., C. W. Ho, J. L. Horwitz, N. Singh, and T. E. Moore, **A new kinetic model for time-dependent polar plasma outflow: Initial results**, Geophys. Res. Lett., 17, 263, 1990.

Yasseen, F., et al., **Monte-Carlo modeling of polar wind photoelectron distributions with anomalous heat flux**, Geophys. Res. Lett., 16, 1023-1026, 1989.

Yau, A. W., E. G. Shelley, W. K. Peterson, and L. Lenchyshy, **Energetic auroral and polar ion outflow at DE-1 altitude, magnitude, composition, magnetic activity dependence a long-term variations**, J. Geophys. Res., 90, 8417, 1985.

Yau, A. W., Andre, M., **Sources of ion outflow in the high latitude ionosphere**, Space Sci. Rev., 80 (1-2), 1-26, 1997.

Yau, A. W., T. Abe, and W. K. Peterson, **The Polar Wind: Recent Observations**, J. Geophys. Res., 90, 8417, 1985, 2007.

Some important references:

Bellan P. M., **Fundamentals of Plasma Physics**, 2004.

Caroline Rayner et al., **Philip's Astronomy encyclopedia**, 2002.

Chen F. F., **Introduction to plasma physics and controlled fusion, 2nd ed**, 1984.

Elkins-Tanton L. T., **The solar system: the sun, Mercury, and Venus**, 2006.

Lucy-Ann McFadden, Paul R. Weissman and Torrence V. Johnson, **Encyclopedia of the solar system**, second edition, 2007.

Michael C. Kelley et al., **The Earth's Ionosphere, Plasma Physics and Electrodynamics**, Second Edition, 2009.

Per Even Sandholt et al., **dayside and polar cap Aurora**, 2004.

Plasma Astrophysics, Fundamentals and Practice, Astronomical Institute and Faculty of Physics, Moscow State University, Springer 2006.

Solar and Space Physics Survey Committee, **The Sun to the Earth -- and Beyond: Panel Reports**, Committee on Solar and Space Physics, National Research Council, 2003.

Internet sources

http://www.solarphysics.kva.se

http://cnx.org

ملخص :

في طبقات الجو العليا على ارتفاع (5000 كم) تتدفق و تتسارع الايونات الموجبه للاعلى مثل ايونات الهيدروجين و الاكسجين و الهيليوم على طول خطوط المجال المغناطيسي, هذه الظاهرة من اهم الظواهر المتعلقة بتاثير الشمس على غلاف الارض الايوني و المغناطيسي , و ينتج عن هذا التفاعل الارض – شمسي مناطق من التدفق الايوني (البلازما) من طبقة الايونوسفير الى طبقة الماغنيتوسفير, يحدث هذا على ارتفاعات كبيرة و على دوائر العرض القريبة من القطبين الشمالي و الجنوبي في ظاهرتين الاولى تدعى الشفق القطبي اوروا (Aurora) و الثانية رياح البلازما القطبية (Polar wind), ان دراسة هذه الظاهرة تزيد من فهمنا لسلوك الايونات في هذه الظروف و يعمق فهمنا لفيزياء بلازما الفضاء, ان الية تسريع الايونات و زيادة طاقتها موضوع نقاش منذ عقود و تدور حوله عدة فرضيات من اهمها فرضية التسخين المعامد للمجال المغناطيسي الناتج عن تفاعل الايونات مع طيف كهرومغناطيسي , ان دراستنا لسلوك الايونات هي متخصصة في منطقة الرياح القطبية (Polar Wind), و قد قمنا باختيار ايونات الهيدروجين H^+ للدراسة بسبب نسبة تواجدها الكبير في منطقة رياح البلازما القطبية, ان الية التسخين المعامد للمجال المغناطيسي الارضي تناولتها عدة نماذج مثل نموذج البرغوثي (Barghouthi), بورام (Bouhram) و ريترر (RCC), لقد قمنا باعطاء النتائج اعتمادا على طريقة مونتكارلو في التحليل Monte Carlo Method, ثم قمنا بالمقارنة بين النتائج في المنطقة القطبية لجميع النماذج , وقمنا ايضا بالمقارنة بين نتائجنا و نتائج النماذج في منطقة الاوروا .